CORONAVIRUS

A multi-specific, multi-affinity antibody platform neutralizes sarbecoviruses and confers protection against SARS-CoV-2 in vivo

Clare Burn Aschner[1]†, Krithika Muthuraman[1,2]†, Iga Kucharska[1], Hong Cui[1], Katherine Prieto[1], Manoj S. Nair[3], Maple Wang[3], Yaoxing Huang[3], Natasha Christie-Holmes[4], Betty Poon[4], Jessica Lam[4], Azmiri Sultana[4], Robert Kozak[5,6], Samira Mubareka[5,6,7], John L. Rubinstein[1,2,8], Edurne Rujas[1,9,10,11], Bebhinn Treanor[12,13,14], David D. Ho[3,15,16], Arif Jetha[1], Jean-Philippe Julien[1,2,12]*

Severe acute respiratory syndrome coronavirus 2 (SARS-CoV-2), the causative agent of coronavirus disease 2019 (COVID-19), has been responsible for a global pandemic. Monoclonal antibodies (mAbs) have been used as antiviral therapeutics; however, these therapeutics have been limited in efficacy by viral sequence variability in emerging variants of concern (VOCs) and in deployment by the need for high doses. In this study, we leveraged the multi-specific, multi-affinity antibody (Multabody, MB) platform, derived from the human apoferritin protomer, to enable the multimerization of antibody fragments. MBs were shown to be highly potent, neutralizing SARS-CoV-2 at lower concentrations than their corresponding mAb counterparts. In mice infected with SARS-CoV-2, a tri-specific MB targeting three regions within the SARS-CoV-2 receptor binding domain was protective at a 30-fold lower dose than a cocktail of the corresponding mAbs. Furthermore, we showed in vitro that mono-specific MBs potently neutralize SARS-CoV-2 VOCs by leveraging augmented avidity, even when corresponding mAbs lose their ability to neutralize potently, and that tri-specific MBs expanded the neutralization breadth beyond SARS-CoV-2 to other sarbecoviruses. Our work demonstrates how avidity and multi-specificity combined can be leveraged to confer protection and resilience against viral diversity that exceeds that of traditional monoclonal antibody therapies.

INTRODUCTION

Emerging infectious agents, including viruses such as severe acute respiratory syndrome coronavirus 2 (SARS-CoV-2), present enormous challenges to global public health through the lack of pre-existing immunity in the population. Despite the availability of vaccines against the disease caused by SARS-CoV-2, the causative agent of coronavirus disease 2019 (COVID-19), global vaccine coverage remains low, with only 29.3% of people in low-income countries having received at least one dose (*1*). Relatively short-lived vaccine-mediated protection, coupled with the emergence of new viral variants, further highlights the necessity for effective prophylactic and treatment options (*2*–*10*). Monoclonal antibodies (mAbs), which have been efficacious in the treatment of infectious diseases, including respiratory syncytial virus (RSV) (*11*) and Ebola virus (*12*), present a promising option. Some mAbs, including bamlanivimab and etesevimab delivered together (*13*), and the REGEN-COV cocktail of casirivimab and imdevimab (*14*), received U.S. Food and Drug Administration (FDA) authorization to treat COVID-19 but have struggled to overcome viral diversity and are limited by the requirement for high doses and intravenous administration (*15*). Both combinations had their authorization revoked after the emergence of the Omicron BA.1 variant of concern (VOC), which has 37 mutations within the spike and 15 mutations within the receptor binding domain (RBD), the target of most clinical antibodies against SARS-CoV-2 (*16*). Furthermore, with the rise of Omicron BQ.1.1 and XBB.1 subvariants, even mAbs that were capable of neutralizing the original Omicron VOC, including bebtelovimab (*17*, *18*), and a cocktail of tixagevimab and cilgavimab (*19*, *20*) have had their authorization revoked because of viral escape (*21*). Despite these limited authorizations, a number of additional antibodies targeting SARS-CoV-2 spike epitopes, including some with broad neutralization against sarbecoviruses, have been identified (*22*–*29*). However, such increases in mAb breadth are often associated with a reduction in potency (*26*), highlighting the necessity of identifying therapeutics that combine potency and breadth.

[1]Program in Molecular Medicine, Hospital for Sick Children Research Institute, Toronto, ON M5G 0A4, Canada. [2]Department of Biochemistry, University of Toronto, Toronto, ON M5S 1A8, Canada. [3]Aaron Diamond AIDS Research Center, Columbia University Vagelos College of Physicians and Surgeons, New York, NY 10032, USA. [4]Combined Containment Level 3 Unit, University of Toronto, Toronto, ON M5S 1A8, Canada. [5]Department of Laboratory Medicine and Molecular Diagnostics, Division of Microbiology, Sunnybrook Health Sciences Centre, Toronto, ON M4N 3M5, Canada. [6]Biological Sciences, Sunnybrook Research Institute, Toronto, ON, Canada. [7]Division of Infectious Diseases, Sunnybrook Health Sciences Centre and Department of Medicine, University of Toronto, Toronto, ON M4N 3M5, Canada. [8]Department of Medical Biophysics, University of Toronto, Toronto, ON M5G 1L7, Canada. [9]Ikerbasque, Basque Foundation for Science, 48013 Bilbao, Spain. [10]Pharmacokinetic, Nanotechnology and Gene Therapy Group, Faculty of Pharmacy, University of the Basque Country UPV/EHU, 01006 Vitoria, Spain. [11]Bioaraba, Microbiology, Infectious Disease, Antimicrobial Agents, and Gene Therapy, 01006 Vitoria, Spain. [12]Department of Immunology, University of Toronto, ON M5S 1A8, Canada. [13]Department of Cell and Systems Biology, University of Toronto, ON M5S 3G5, Canada. [14]Department of Biological Sciences, University of Toronto Scarborough, Toronto, ON M1C 1A4, Canada. [15]Department of Microbiology and Immunology, Columbia University Vagelos College of Physicians and Surgeons, New York, NY 10032, USA. [16]Division of Infectious Diseases, Department of Medicine, Columbia University Vagelos College of Physicians and Surgeons, New York, NY 10032, USA.
*Corresponding author. Email: jean-philippe.julien@sickkids.ca
†These authors contributed equally to this work.

Increasing antibody valency is a promising approach to enhancing apparent binding affinity (*30*–*32*), potentially lowering therapeutic dose, improving breadth, and allowing administration through alternative routes, such as subcutaneous or intramuscular delivery. Aiming to exploit avidity to enhance antibody functional responses, a wide range of antibody engineering strategies have been described (*33*). Among those, biologics assembled based on immunoglobulin G (IgM) (*34*), synthetic nanocages (*35*), and minibinder (*36*) formats have demonstrated superior neutralization properties against SARS-CoV-2 compared with conventional mAb formats. In addition, the avid molecules GEN3009 (*37*), INBRX-106 (Inhibrx) (*38*), and IGM-8444 (*39*) are being tested in phase 1/2 clinical trials for the treatment of hematological and solid tumors, highlighting the clinical benefit of multivalent antibody-presenting formats. Following a similar principle, but using the human light-chain apoferritin protomer to drive oligomerization of antibody fragments, we developed a platform called the Multabody (MB) to increase neutralization potency of antibodies targeting SARS-CoV-2 (*40*) and HIV-1 (*41*). Using this platform, enhanced affinity can be coupled with multi-specificity—the inclusion of several antibody fragments recognizing different epitopes—to result in antigen recognition that is more resistant to viral mutations (*40*, *41*). This is particularly relevant in light of immune pressure driving the continued emergence of new variants of SARS-CoV-2, including those against which existing vaccines and drugs are less efficacious (*42*–*44*).

Here, we explored whether the increased in vitro SARS-CoV-2 neutralization previously reported for the MB could translate to in vivo protection at low doses. In addition, we assessed whether MBs could rescue the loss in neutralization potency observed for conventional mAbs against different VOCs and expand breadth beyond SARS-CoV-2. Our data provide proof of concept that the MB is a tractable platform that harnesses avidity to provide gains in both the in vitro and in vivo potency and breadth of antibody-based molecules against SARS-CoV-2 and other coronaviruses.

RESULTS

The tri-specific 298-52-80 MB adopts its intended structural disposition

We have previously reported the generation of tri-specific MB molecules using an engineered apoferritin split design (Fig. 1A) (*40*, *41*), whereby the human apoferritin protomer was split into two halves on the basis of its four-helical bundle fold: the two N-terminal α helices (N-Ferr) and the two C-terminal α helices (C-Ferr). The genetic fusion and transfection into mammalian cell expression systems of a single-chain (sc) Fab or an scFc at the N terminus of each apoferritin half and full apoferritin resulted in the secretion of self-assembled, oligomeric molecules capable of ultrapotent neutralization. Specifically, a tri-specific MB incorporating Fabs derived from mAbs 298, 52, and 80 increased neutralization potency by about 1000-fold compared with the corresponding IgG cocktail (*40*). This tri-specific MB was described to have antibody-like biochemical properties, as assessed in biophysical characterizations after purification and under accelerated thermal stress (*40*). To obtain molecular insights into the assembly of the MB design, we next characterized this tri-specific MB by cryo–electron microscopy (cryo-EM) (fig. S1).

Analysis of cryo-EM micrographs revealed the formation of highly decorated and homogeneous nanocage-like particles (Fig. 1B). Consistent with the presence of flexible $(GGS)_x$ linkers connecting the scFab and scFc components to the apoferritin scaffold, the density of these antibody fragments is poorly resolved in two-dimensional (2D) classes (Fig. 1C) and 3D reconstruction of the tri-specific MB (Fig. 1D). However, manual picking of the scFab and scFc particles, followed by template-based particle picking, and subsequent refinement of these molecules confirmed the proper assembly of Fab and Fc components on the MB to about 7 Å resolution (Fig. 1, B to D, and figs. S1 and S2).

Three-dimensional reconstructions of the apoferritin scaffold of the MB reached 2.4 and 2.1 Å resolution, respectively, when no symmetry (C1; Fig. 1D and fig. S3, A to D) or octahedral symmetry (O; fig. S3, E to H) was applied. The apoferritin scaffold in the tri-specific MB is virtually identical to that of the human apoferritin light chain [Protein Data Bank (PDB) ID: 6WX6], with measured cross-correlation coefficients between maps of 0.97 (C1) and 0.92 (O). The N and C termini of the core MB scaffold are similarly disposed in three- and fourfold symmetry axes as in the native human apoferritin light chain (Fig. 1D), indicating minimal impact for scFab and scFc genetic fusions. Data collection from a mixture of "split" and "nonsplit" apoferritin units within the MB results in the averaging of the split design site to closely resembles the nonsplit apoferritin monomer, and the cryo-EM maps showed no evidence of deviation from the apoferritin fold for structural elements at the split design site (between residues Trp^{93} and Gly^{94}; Fig. 1D, bottom right, red arrow). In summary, our cryo-EM analysis of the tri-specific 298-52-80 MB provided atomic-level details demonstrating that the MB, built on the apoferritin split design scaffold, adopted its intended structural disposition.

Neutralization potency correlates with in vivo protection from SARS-CoV-2

Next, we investigated the ability of the tri-specific 298-52-80 MB to confer in vivo protection against SARS-CoV-2. To specifically assess the effect of neutralization potency on in vivo protection from lethal SARS-CoV-2 challenge, we generated a tri-specific 298-52-80 MB and the corresponding IgG cocktail with an IgG4 Fc containing mutations (S228P, F234A, L235A, G237A, and P238S) (*45*) to ablate binding to Fcγ receptors (FcγRs), hereafter referred to as MB* and IgG4*, respectively. As expected, replacement of the Fc subtype from IgG1 to IgG4* did not affect the neutralization potency of the IgG or the MB, as previously reported (*40*). The tri-specific MB* achieved a half-maximal inhibitory concentration (IC_{50}) value of 0.0002 μg/ml, about 1000-fold more potent than its corresponding cocktail IgG (Fig. 2A). Binding kinetics studies revealed that both the tri-specific MB* and the IgG4* antibody cocktail displayed pH-dependent binding to mouse and human neonatal Fc receptor (FcRn) (Fig. 2, B and C) and no binding to human and mouse FcγR. This was in contrast to the FcγR binding observed for the corresponding IgG1 antibody cocktail control (Fig. 2C and fig. S4, A and B). The MB* and IgG4* antibody cocktail also displayed no binding to mouse and human FcRn at physiological pH and binding at acidic pH with no detectable off rate (fig. S4, A and B). Antibody-dependent cell-mediated phagocytosis (ADCP) experiments using fluorescently labeled beads coated with SARS-CoV-2 spike protein further confirmed the inability of the tri-specific MB* and the IgG4* cocktail to engage Fc receptors, whereas the

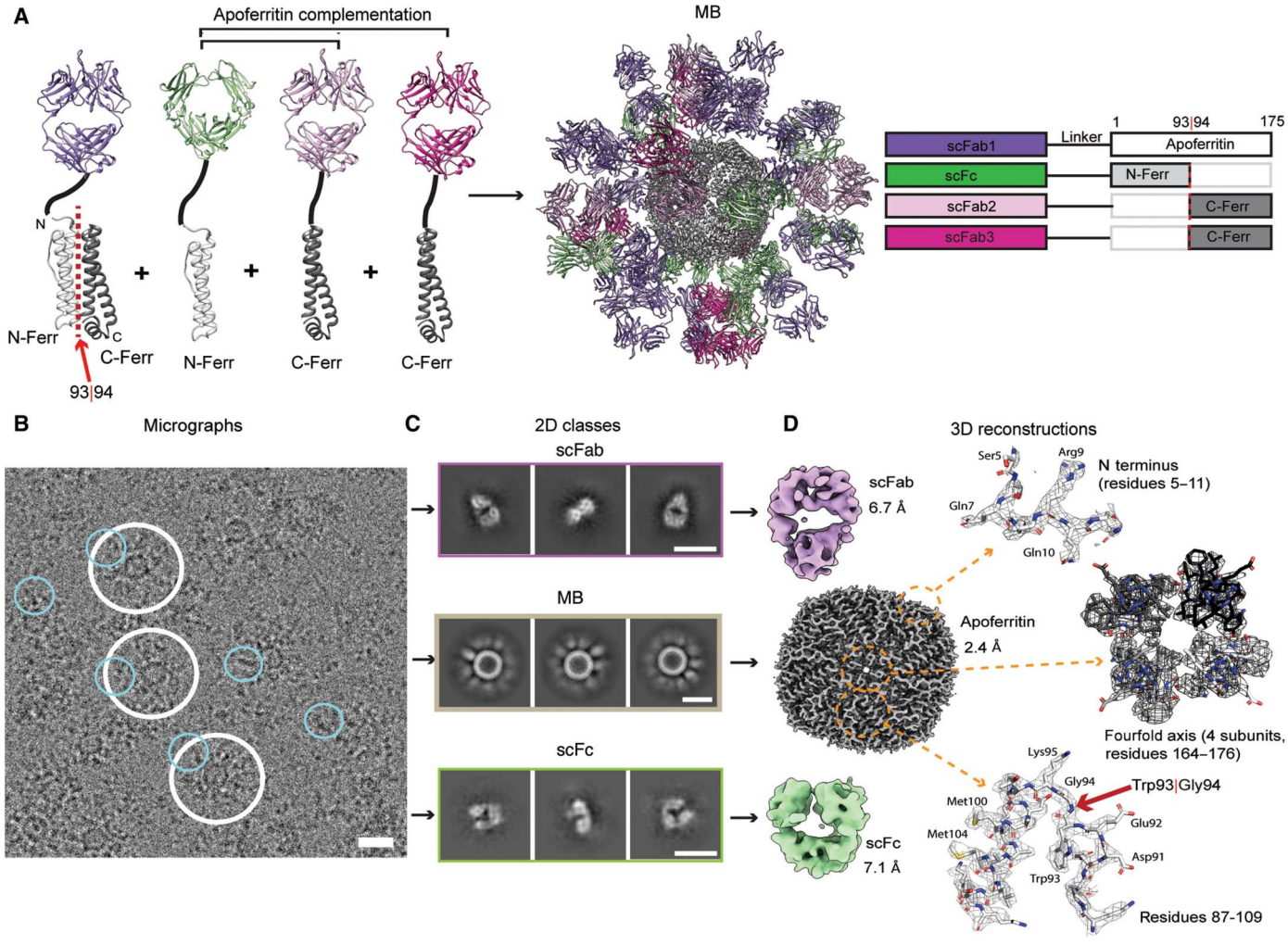

Fig. 1. cryo-EM characterization of the tri-specific MB. (**A**) Schematic representation of the elements that drive assembly of the tri-specific MB (298-52-80). The red arrow indicates the split site between the first half (N-Ferr) and the second half (C-Ferr) of the human apoferritin light chain. (**B**) Representative cryo-EM micrograph of the tri-specific MB with white and cyan circles highlighting the whole particles and scFab/scFc fragments, respectively. (**C**) Representative 2D classes of scFab (top), tri-specific MB (middle), and Fc domains (bottom). (**D**) The left panels show cryo-EM maps of scFab at 6.7 Å resolution (top), apoferritin nanocage scaffold at 2.4 Å resolution (middle), and scFc at 7.1 Å resolution (bottom). The right panels show fitting of the human apoferritin light-chain model (PDB ID:6WX6) into the 2.4 Å map, focusing on features such as the N terminus of the apoferritin scaffold. The map shows weak density beyond Ser^5 due to the flexibility of the linker (top), the four-fold axis formed by four adjacent subunits (middle), and residues 87 to 109 of the human apoferritin light chain (bottom). The red arrow points to the split site, between residues Trp^{93} and Gly^{94} in some subunits. All cryo-EM maps in this figure were refined with no symmetry applied. Scale bars, 10 nm.

IgG1 antibody cocktail showed substantial uptake of SARS-CoV-2 spike protein-coated beads (Fig. 2D and fig. S4C).

To assess whether the increased neutralization potency achieved with the MB resulted in improved in vivo protection against SARS-CoV-2, human angiotensin-converting enzyme 2 (hACE2) and human FcRn (hFcRn) double-transgenic mice were treated with 30 μg (1.5 mg/kg) of the FcγR binding–deficient IgG4* and MB* molecules and challenged intranasally with a high dose of 1×10^5 50% tissue culture infectious dose ($TCID_{50}$) of SARS-CoV-2 (*46*). The tri-specific MB* provided significantly better protection (60% survival, $P < 0.0001$) compared with the IgG4* cocktail, with all cocktail-recipient animals succumbing to the challenge at days 6 to 7 after challenge (Fig. 2E). Improved protection was associated with reduced weight loss and weight rebound after challenge (fig. S4D), fewer clinical signs of disease throughout the course of infection (fig. S4E), and significantly ($P < 0.0001$) lower lung viral titers, particularly in animals that survived the challenge (Fig. 2F). Infection was confirmed by reverse transcription quantitative polymerase chain reaction using oropharyngeal swabs collected at day −1 (before challenge) and day 2 after challenge (fig. S4F). In subsequent studies, we found that comparable in vivo protection was achieved when the tri-specific MB* was delivered at 3 μg (1.4 pmol; 0.15 mg/kg) and the IgG4* cocktail at 90 μg (600 pmol; 4.5 mg/kg) (Fig. 2G). The difference in dose can be observed in circulating serum concentrations of administered molecules at day 2 after challenge (Fig. 2H). These data not only provide evidence of in vivo protection from lethal challenge mediated by the MB but also illustrate that the increased neutralization potency conferred by the tri-specific MB* format provides enhanced protection against SARS-CoV-2 challenge compared with a corresponding IgG mixture.

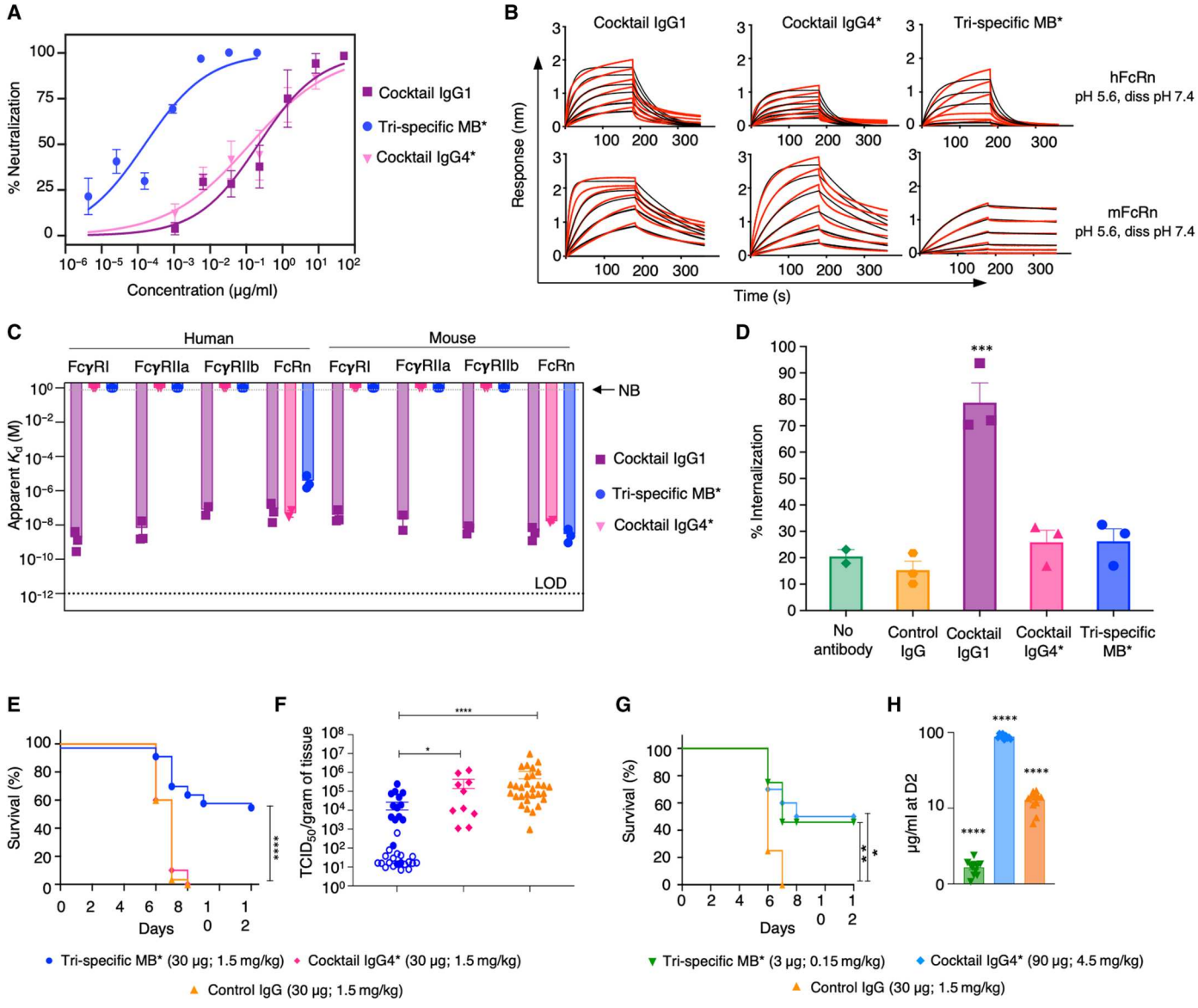

Fig. 2. MBs protect against SARS-CoV-2 challenge. (**A**) SARS-CoV-2 PsV neutralization potency of the tri-specific (289-52-80) MB* and the corresponding IgG1 and IgG4 cocktails. * indicates the use of IgG4 Fc bearing mutations (S228P, F234A, L235A, G237A, and P238S) that ablate FcγR binding. (**B**) Sensograms of samples shown in (A) binding to human and mouse FcRn (association at pH 5.6 and dissociation at pH 7.4). (**C**) Binding [apparent K_d (dissociation constant)] of cocktail IgG1, cocktail IgG4*, and tri-specific MB* particles to human (FcγRI, FcγRIIa, FcγRIIb, and FcRn) and mouse (FcγRI, FcγRIIb, FcγRIV, and FcRn) Fc receptors. NB and LOD denote no binding and limit of detection, respectively. (**D**) ADCP was determined as the percentage of THP-1 cells with internalized SARS-CoV-2 spike protein–coated fluorescent microspheres. (**E** and **F**) Mice expressing hACE2 and hFcRn were dosed (30 μg; 1.5 mg/kg) as indicated and challenged intranasally with 1×10^5 plaque-forming units of SARS-CoV-2 per mouse. (E) Survival was monitored for 12 days after challenge. (F) Lung viral titers at the end of the experiment (open symbols) or at the time of death in the animals that succumbed (closed symbols) were measured by viral outgrowth assay. $TCID_{50}$ per gram of tissue is shown. (**G** and **H**) Mice were inoculated as in (E) and (F) and treated with a lower dose of tri-specific MB* [3 μg (1.4 pmol); 0.15 mg/kg]. Survival (G) and serum IgG or MB concentrations at day 2 (H) after administration of low-dose tri-specific MB* are shown compared with high-dose cocktail IgG4* [90 μg (600 pmol); 4.5 mg/kg]. Means ± SD (A, C, and D) and representative data (B) for at least three independent experiments are shown. In (E) and (F), $n = 33$ for tri-specific MB*, $n = 30$ for control IgG, and $n = 10$ for cocktail IgG4*; data are from two to six independent experiments. In (G and H), $n = 24$ for tri-specific MB*, $n = 10$ for cocktail IgG4* mix, and $n = 8$ for control IgG; data are from two to five independent experiments. For (D), *** indicates significance compared with no antibody control ($P < 0.001$) by analysis of variance (ANOVA). For (E), ****$P < 0.0001$ by Gehan Breslow Wilcoxon test. For (F), ****$P < 0.0001$ and *$P < 0.05$ by Kruskal-Wallis test. For (G), *$P < 0.05$ and **$P < 0.001$ by Gehan Breslow Wilcoxon test. For (H), ****$P < 0.0001$ compared with all other groups by ANOVA.

MBs display enhanced potency and breadth against SARS-CoV-2 VOCs

Since the early discovery of mAbs 298, 52, and 80 in 2020, extensive research efforts worldwide have focused on the identification of potent antibodies against SARS-CoV-2 (*47*). In this context, 2-7 (*48*), 2-36 (*25*), 2-38 (*48*), 10-40 (*49*), and 11-11 (*49*) have emerged as RBD-binding mAbs displaying both potency and breadth against SARS-CoV-2 and its variants. To assess whether the neutralization properties of these mAbs could be further improved, we expressed mono-specific MBs and evaluated their neutralization potency and breadth compared with their corresponding mAbs against SARS-CoV-2 wild-type (WT) and five VOCs (Alpha, Beta, Gamma, Delta, and Omicron BA.1). Five of the eight mAbs (52, 80, 2-36, 11-11 and 10-40) showed 100% breadth with an IC_{50} cutoff value of 5 μg/ml. However, when using an IC_{50} cutoff value of 0.01 μg/ml to resemble the potency of REGEN-COV (*50*), only two mAbs (11-11 and 10-40) showed neutralization against two of the five VOCs tested (Fig. 3A and fig. S5). In contrast, when displayed as mono-specific MBs, three specificities (2-7, 80, and 52) reached 100% neutralization breadth using an IC_{50} cutoff value of 0.01 μg/ml. The remaining MBs lose potency against Omicron BA.1 but, apart from 298 and 2-38 MBs, still neutralize with an IC_{50} below 0.3 μg/ml, the pseudo-virus (PsV) neutralization potency of sotrovimab (*51*) against WT SARS-CoV-2 (Fig. 3, B and C, and fig. S5). The superior ability of these molecules to overcome viral sequence diversity is likely due to their enhanced potency against WT SARS-CoV-2, which ranges from 0.005 to 0.0002 μg/ml (Fig. 3B). These increases in potency and breadth were not associated with increases in binding to antigens commonly used as measures of polyreactivity, namely, cardiolipin, insulin, double-stranded DNA, and keyhole limpet antigen (fig. S6).

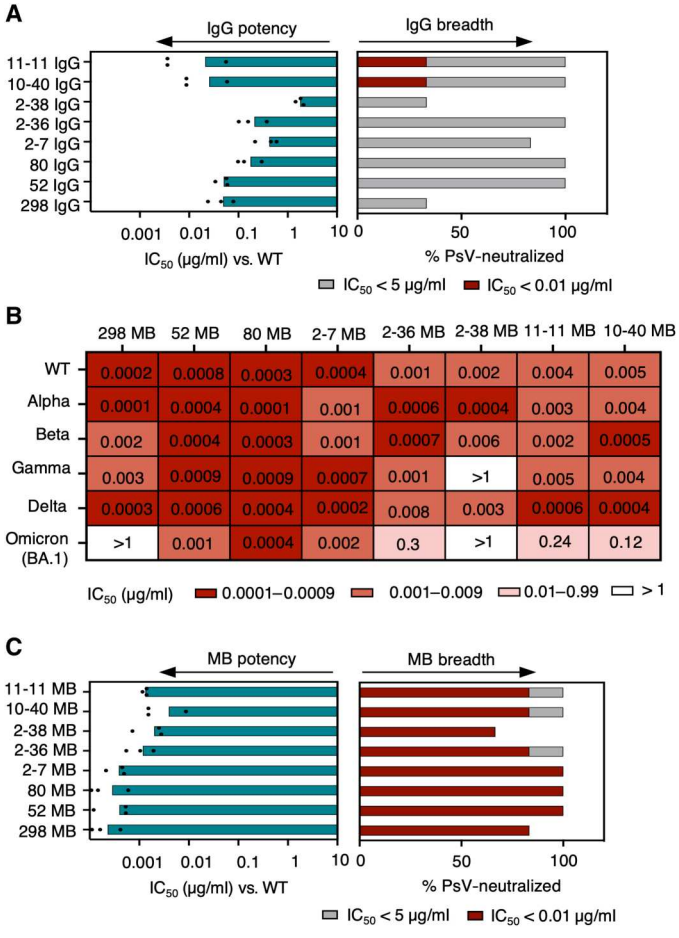

Fig. 3. MBs are potent and broad SARS-CoV-2 neutralizers. (**A**) IgG neutralization potency (teal bars) and breadth are shown against a six PsV panel using a cutoff IC_{50} value of 5 μg/ml (gray bars) or 0.01 μg/ml (red bars). (**B**) Heatmap showing the neutralization potency of mono-specific MBs displaying Fab specificities from (A) against each PsV variant in the panel. Individual IC_{50} values are displayed. (**C**) Neutralization potency and breadth of mono-specific MBs are shown as in (A). The PsV panel includes WT, Alpha, Beta, Gamma, Delta, and Omicron BA.1. Data from three biological replicates are shown, and bars indicate the means.

The MB format can confer resilience to overcome antigenic shift even when antibody interacts with mutated residues

Next, we sought to understand the molecular basis of binding of mAb 80, because its structure had remained elusive. We solved the crystal structure of 80 Fab in complex with the RBD at 3.1 Å resolution (Fig. 4A, fig. S7, and table S1). Epitope recognition is mediated by 20 residues that form the interface with the RBD, 14 of which are involved in ACE2 binding (table S2). This illustrates how mAb 80 inhibits SARS-CoV-2 infection through receptor blockade, preventing the interaction of ACE2 with the receptor binding motif (Fig. 4A). The heavy chain of mAb 80 is primarily responsible for the interaction with the RBD, contributing 10 of the 11 hydrogen bonds found in the binding interface (fig. S8, A and B, and table S2). In addition, interaction of F54 of the antibody heavy chain with Y489 from the RBD results in the formation of a new triple pi-stacking within the RBD structure, between residues Y473, F456, and Y421 (fig. S8C).

Detailed analysis of the RBD–80 Fab interface revealed that residues S477 and T478 of the RBD form hydrogen bonds with Y^{92} and D^{100D} of the antibody, burying 124 $Å^2$ of its surface area and accounting for 15% of the total buried surface area (BSA) of the RBD (Fig. 4, B and C, and table S2). These residues are mutated in several VOCs, including Omicron (BA.1 and BA.2), which reduces the binding affinity of the antibody to the Omicron BA.1 RBD (Fig. 4, D and E); however, the increased avidity achieved with the MB format compensates for this weaker binding. Consequently, the interaction of 80 MB with the mutated Omicron BA.1 RBD has a high apparent binding affinity with no detectable off-rate (Fig. 4, D and E), which likely contributes to resilient neutralization potency against Omicron BA.1 (Fig. 3B). The potency of the 80 MB against Omicron BA.2 was additionally confirmed using the replication-competent virus. As expected, considerably reduced potency against Omicron BA.2 live virus is observed for the 80 mAb, but high neutralization potency is retained in the MB format (Fig. 4F).

A tri-specific MB broadly neutralizes sarbecoviruses.

Although mono-specific MBs show potent neutralization and can rescue loss in potency compared with their mAb counterparts, mono-specificity still carries the risk of viral escape should sufficient mutations emerge to overcome the benefit conferred by binding avidity. The 80 mono-specific MB loses neutralization against Omicron BA.5 (fig. S9A), highlighting the need for an improved approach to tackling evolving viral variants and achieve exquisite neutralization breadth that could potentially also extend to other

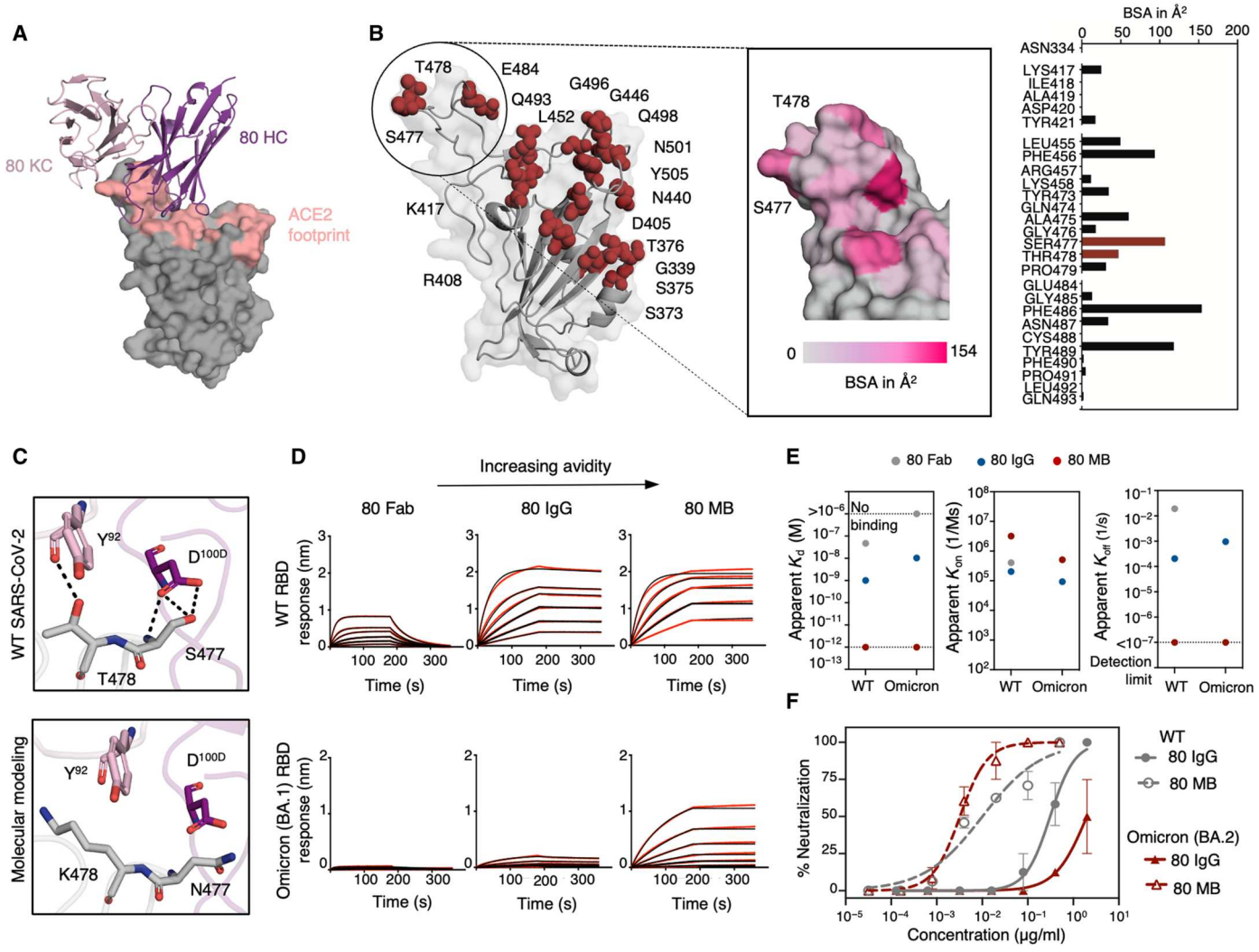

Fig. 4. The MB format confers resilient SARS-CoV-2 neutralization despite viral evolution. (**A**) Three-dimensional structure of the 80 Fab–RBD complex. The heavy and kappa light chains (HC and KC, respectively) of 80 Fab are colored in dark and light purple, respectively. RBD is shown as surface representation (gray), with the footprint of ACE2 depicted in salmon. (**B**) Secondary structure cartoon representation of RBD, with residues mutated in the different variants of concern highlighted as red spheres. Inset: Close-up view of the RBD area recognized by 80 Fab. Critical residues for binding are colored in pink according to their BSA. Mutated residues in the VOCs are indicated and shown in red in the BSA plot. (**C**) Molecular modeling displays the possible conformation adopted by the side chains of the mutated RBD residues T478K and S477N (gray) upon 80 Fab (pink) binding. Hydrogen bonds are shown as dashed black lines. (**D**) Sensograms of 80 Fab, 80 IgG, and 80 MB binding to WT and Omicron BA.1 RBD. Red lines represent raw data, and black lines represent global fit. (**E**) Comparison of the binding kinetic parameters of 80 as a Fab, IgG, and MB for binding to WT and Omicron BA.1 RBDs. The data shown are averages from two independent experiments. The dotted horizontal lines indicate the LOD. (**F**) Authentic virus neutralization of 80 IgG and 80 MB against WT and Omicron BA.2 is indicated in gray and red, respectively. The means ± SD for two technical replicates are shown in each neutralization plot.

sarbecoviruses beyond SARS-CoV-2. On the basis of this and the results from the mono-specific MB screening (Fig. 3B), we chose mAb specificities 2-7, 10-40, and 11-11 to design a tri-specific molecule to explore neutralization gains made by combining next-generation mAbs of different epitope specificities on the MB. Similar to mAb 80, previous structural data on mAb 2-7 revealed that RBD mutations found in VOCs form part of its binding interface (fig. S9, B and C) (*52*), leading to the neutralization potency loss observed for this IgG against Omicron BA.1. However, 2-7 binding and neutralization potency were rescued in the MB format (Fig. 5A and fig. S9, D and E), including potent neutralization against Omicron BA.5 (fig. S9A), demonstrating again the benefit of avidity to overcome viral escape. mAbs 10-40 and 11-11 have been shown to target conserved epitopes on the RBD and consequently confer broad neutralization that expands to other sarbecoviruses (*49*).

The resulting tri-specific (2-7–10-40–11-11) MB potently neutralized WT and six SARS-CoV-2 VOCs (Alpha, Beta, Gamma, Delta, Omicron BA.1, and Omicron BA.5) in PsV neutralization assays, with a mean IC_{50} of 0.002 μg/ml (Fig. 5B and fig. S10A). These experiments were expanded using other viruses dependent on ACE2 as an entry receptor, including live Omicron BA.2 virus and a SARS-CoV-1–related bat sarbecovirus panel. To better assess the benefit of combining multi-specificity, the mono-specific

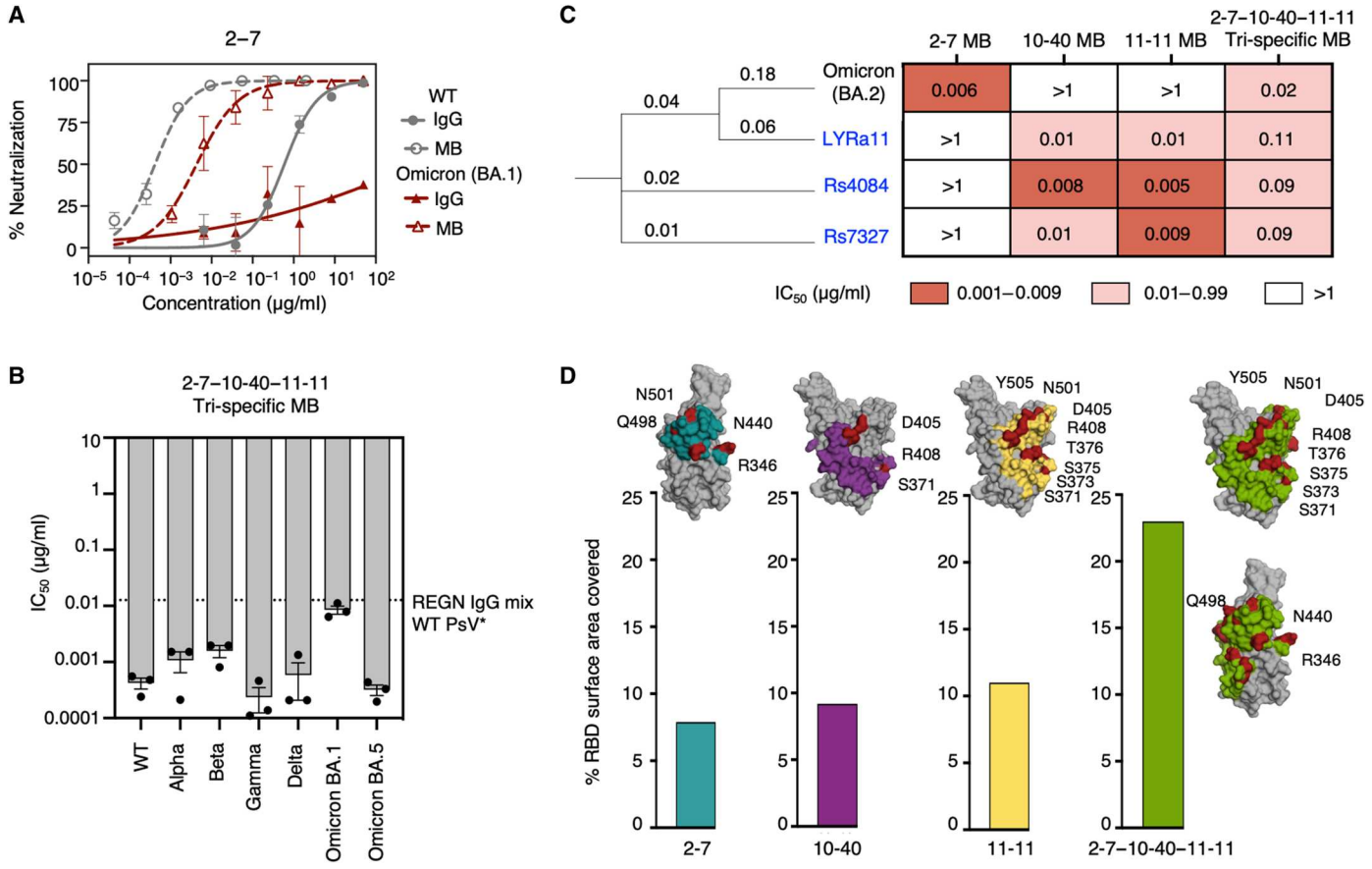

Fig. 5. A tri-specific MB potently and broadly neutralizes sarbecoviruses. (**A**) PsV virus neutralization of 2-7 IgG (solid line) and 2-7 MB (dashed lines) against WT (gray) and Omicron (BA.1, red). The means ± SD for two technical replicates are shown in each neutralization plot. (**B**) Neutralization potency (gray bars) and breadth of the 2-7–10-40–11-11 tri-specific MB against SARS-CoV-2 PsV and six VOCs are shown. *The dashed line indicates IC_{50} of the REGN IgG mix against WT SARS-CoV-2 PsV. (**C**) Shown is a phylogenetic tree with branch lengths representing sarbecovirus divergence. The heatmap shows the neutralization potency of the 2-7–10-40–11-11 tri-specific MB and its corresponding monospecific MBs against Omicron (BA.2) live virus and three SARS-CoV-1–related bat coronaviruses' (labeled in blue) PsVs. Individual IC_{50} values are shown. (**D**) Bar graphs indicating the percentage accessible surface area on the RBD (gray) covered by the tri-specific MB (green) and respective components, 2-7 (teal) (PDB ID: 7LSS), 10-40 (purple) (PDB ID: 7SD5), and 11-11 (yellow) (EMD: 25167). Mutations found in SARS-CoV-2 VOCs [Alpha, Beta, Gamma, Delta, and Omicron (BA.1, BA.2)] that are part of each antibody binding interface are shown in red.

MB components were also tested. The mono-specific 2-7 MB did not show neutralization against the sarbecovirus panel, whereas 10-40 and 11-11 MBs were not able to block infection of live Omicron BA.2 (Fig. 5C and fig. S10, B and C). In contrast, the tri-specific MB of these specificities combined on a single molecule displayed both potent SARS-CoV-2 neutralization across the VOCs, including live Omicron BA.2, and pan-sarbecovirus neutralization of this panel (Fig. 5, B and C, and fig. S10, A to C). We further tested the 2-7–10-40–11-11 tri-specific MB and the corresponding IgG cocktail against the recent BQ.1.1 and XBB.1 Omicron subvariants to assess potency in PsV neutralization assays. The potency of the IgG cocktail falls below the IC_{50} range of clinically authorized antibodies [0.3 μg/ml, sotrovimab (*51*) and 0.01 μg/ml, REGEN-COV (*50*) against WT SARS-CoV-2 PsV] and does not reach 100% neutralization even at 100 μg/ml (fig. S10, D and E). In contrast, the tri-specific MB neutralized the BQ.1.1 and XBB.1 subvariants at a potency of 0.06 and 0.18 μg/ml, respectively, which still falls within the dosing range of FDA-authorized therapeutics against WT SARS-CoV-2 (fig. S10, D and E).

To gain insight into the molecular coverage of the tri-specific 2-7–10-40–11-11 MB, we analyzed the individual and combined RBD BSA of each antibody specificity on the basis of their previously published three-dimensional structures. Binding of mAbs 2-7, 10-40, and 11-11 to the RBD covers about 8, 9, and 11% of the RBD-accessible BSA, respectively, whereas, in the case of the 2-7–10-40–11-11 tri-specific MB, 23% of the RBD accessible BSA is covered with a single molecule (Fig. 5D). Correspondingly, the tri-specific 2-7–10-40–11-11 MB contains 62 contact residues in the RBD compared with 23, 27, and 37 residues in the case of individual mAbs 2-7, 10-40, and 11-11, respectively. Therefore, by targeting three partially overlapping functional epitopes on the RBD, and through the potency gain provided by avidity, the tri-specific 2-7–10-40–11-11 MB provides proof of concept for potent, broad, and resilient neutralization across sarbecoviruses by a single molecule.

DISCUSSION

The rapid emergence of new SARS-CoV-2 VOCs has stymied mAb therapeutics and driven antibody discovery efforts focused on expanding the breadth of viral sequences recognized by a single antibody (*22*, *23*, *53*). The evidence that all FDA-authorized mAb therapies have successively lost efficacy against the Omicron VOC and its subvariants (*16*, *20*, *54*) supports the urgent need for additional therapeutic interventions with improved breadth. In addition, strategies to propel the potency of such mAbs have the potential to reduce the therapeutic dose and enable more practical routes of administration, which could reduce manufacturing costs and enable global availability. We have previously described a MB platform capable of delivering highly potent and broadly acting molecules in vitro (*40*, *41*). Despite being developed from three early-identified mAbs of modest potency, the tri-specific 298-52-80 MB has extremely potent neutralizing activity (IC_{50} of 0.0002 μg/ml). Here, we have demonstrated that potent in vitro neutralization of SARS-CoV-2 translates into in vivo protection at a low dose and that combination of avidity and multi-specificity can yield molecules with broad neutralization coverage against sarbecoviruses.

The MB platform offers multiple advantages as a next-generation multivalent biologic, including high stability, efficient assembly, ease of production and purification, and plug-and-play genetic fusion of antibodies of choice (*40*, *41*). Here, we further confirmed the proper assembly of a tri-specific MB by cryo-EM. This structural technique has been useful for the characterization of large and complex biological designs such as subunit vaccines, including self-assembling protein nanoparticles presenting the ectodomains of influenza and RSV viral glycoprotein trimers (*55*), two-component protein nanoparticles displaying a stabilized HIV-1 Env trimer (*56*), or a COVID-19 vaccine candidate nanoparticle using SpyCatcher multimerization of the SARS-CoV-2 spike protein RBD (*9*). Although simultaneous visualization of both nanoparticle scaffold and molecules displayed at their periphery can be challenging because of the flexibility of linkers, recent advances in cryo-EM data processing allow for independent analysis of different nanoparticle components (*57*, *58*). By adopting this strategy, we were able to confirm the proper folding of scFabs and scFcs at the periphery of the MB. Furthermore, we confirm at 2.1 Å resolution the proper assembly of the human light-chain apoferritin scaffold of the MB in the context of the engineered split design, on which the assembly of multi-specific antibody components is built. These analyses are important because they further support a central role for structure-guided protein engineering in the rational design of biologics and substantiate the MB as a uniform biologic.

Next, we investigated the ability of the MB to confer protection from lethal challenge in vivo. The specific role of increased neutralization potency in mediating in vivo protection was assessed with a tri-specific MB* molecule expressing a mutant IgG4 Fc that is defective for FcγR binding. In attempts to retain IgG-like bioavailability as previously described (*40*), we maintained the ability of the MB Fc to interact with FcRn, a receptor associated with antibody recycling and half-life extension (*59*, *60*). In vivo, the marked increase in neutralization potency of the tri-specific MB relative to the IgG4* cocktail resulted in better protection against the lethal SARS-CoV-2 challenge and facilitated a reduction in the dose required for protection. Comparable in vivo efficacy was obtained with about 430× less molar amount of the MB compared with the IgG. Previous studies have shown that some mAbs targeting SARS-CoV-2 require Fc-mediated effector functions for optimal efficacy (*61*–*65*). Our data illustrate that gains in neutralization potency are sufficient to confer protection from lethal challenge, even in the absence of effector function, and support the use of avidity-based increases in potency to facilitate dose-sparing of antibody-based therapeutics. Further studies will investigate whether MB potency can be further enhanced through the addition of effector functions, by incorporating WT Fc or engineering the Fc to introduce specific functions. We have previously shown that the MB format is capable of triggering ADCP in vitro, indicating that the format itself does not preclude incorporating effector function into the molecule (*41*).

Single-specificity MBs showed an elevated degree of resilience against viral sequence variability through improvements in their apparent binding affinity compared with IgGs, allowing these molecules to retain neutralization capabilities even when mAbs lose potency. Not all Fabs experience an equivalent boost in potency when expressed as a MB, the basis of which is likely attributed to multiple Fab-epitope factors and continues to be investigated in ongoing work. In the case of both mAbs 80 and 2-7, mutations within the RBD epitope found in the VOCs cause a loss in potency by the mAbs. In contrast, when these specificities are displayed as MBs, mutations present in the VOCs minimally alter the high apparent binding affinity and potent neutralization profiles of these molecules. The ability of the MB to better tolerate sequence variability presumably stems from the reduced off-rate that drives increased avidity, which might be favored by the spike density on the virion surface (*66*–*68*). The potential for avid antibody technologies to endure viral sequence variability can provide benefits to antibody discovery timelines by boosting the longevity of early-identified mAbs with the ability to neutralize emerging VOCs without appreciable increases in self-reactivity. Despite these data, we observed that single-specificity avid molecules can have a limit in terms of how much resilience against viral diversity they can provide, as seen by the loss of neutralization potency by the mono-specific 80 MB against the Omicron BA.5 VOC. To overcome this, multiple best-in-class antibodies can be combined into a multi-specific MB to retain even more resilient potency in the face of rapid viral evolution.

The identification of potent broadly neutralizing antibodies can take years or even decades of antibody discovery and engineering efforts, as exemplified in the cases of HIV-1 and influenza. Here, we demonstrate that a tri-specific MB incorporating the specificities 2-7, 10-40, and 11-11 has potent in vitro neutralization across all SARS-CoV-2 VOCs tested, including recent BQ.1.1 and XBB.1 Omicron subvariants, and expand its neutralization breadth to other sarbecoviruses at neutralization potencies within the range of FDA-authorized therapeutics against SARS-CoV-2 (*51*). The continuous monitoring and screening of emerging variants will be required to confirm the persistence of neutralization; however, the larger footprint of the RBD covered by a tri-specific MB compared with conventional mAbs provides a unique advantage for the MBs in remaining resilient against future VOCs compared with mAbs alone. Furthermore, the ability to combine multiple specificities into a single molecule might offer the additional potential benefit of ensuring the bioavailability of all components throughout the course of therapy, which has been a limiting feature of mAb cocktail combinations (*46*, *69*).

Our study has some limitations. Further studies of the pharmacokinetics and tissue distribution of the MBs compared with corresponding cocktails of mAbs in higher-order species will be required to fully evaluate the potential applications of this emerging modality. In time, it will also be important to compare the efficacy of the MB platform with the efficacy of other experimental modalities that harness the power of avidity. The MB is restricted by the rate and quality of antibody discovery, and ongoing efforts will explore the potential of combining the most potent broadly neutralizing antibodies that continue to emerge from discovery efforts on an avid antibody platform to evaluate the full potential of this approach against betacoronaviruses. The MB platform may further present a promising avenue to explore also in the context of other viral pathogens of high genetic diversity to further enhance the breadth and potency of antibody therapeutics against indications of global health importance.

MATERIALS AND METHODS

Study design

The objective of this study was to further validate and develop the use of the MB format to overcome viral diversity through the incorporation of newly identified potent antibodies and to determine whether the MB could provide in vivo protection against SARS-CoV-2 challenge. Correct MB assembly was verified by cryo-EM, and molecular details of Fab interactions with the RBD were determined by x-ray crystallography. Binding was determined by biolayer interferometry. Potency was determined by neutralization assays using PsV or authentic SARS-CoV-2 and sarbecoviruses. In vitro studies of binding and neutralization potency determined which molecules progressed to in vivo testing in mice. Animal sample sizes were determined using power calculations estimating 80% power to detect differences in survival and were based on effect sizes from preliminary studies. Age- and weight-matched animals were randomly assigned to experimental groups by ear tag number, and personnel were blinded to their group assignments during the course of the study. Animals were weighed and monitored daily for signs of disease and sacrificed according to the approved ethical endpoint—lack of provoked movement, rapid breathing, hunching, and reduced grooming or >20% body weight loss. Sample sizes and experimental replicates are indicated in the figure legends.

Cell lines and viruses

Human embryonic kidney (HEK) 293T-ACE2 cells (BEI NR2511), HEK 293T (ATCC, American Type Culture Collection) and VeroE6 (Green Monkey Kidney cell line, ATCC) cells were grown in Dulbecco's modified Eagle's medium (DMEM; Thermo Fisher Scientific). For HEK 293T and HEK 293T-ACE2 cells, DMEM was supplemented with 10% heat-inactivated fetal bovine serum (FBS), 5% 1 M Hepes, and 1% gentamicin (all Thermo Fisher Scientific). For VeroE6 cells, DMEM was supplemented with 10% FBS (HyClone, Logan, UT) and 1% penicillin-streptomycin (Invitrogen, Thermo Fisher Scientific). HEK 293F and HEK 293S cells (Thermo Fisher Scientific) were cultured in FreeStyle 293 Expression Medium (Thermo Fisher Scientific) at 125-rpm oscillation, 37°C, and 8% CO_2. SARS-CoV-2/SB2-P4-PB Clone 1 (*46*) titers were determined by $TCID_{50}$ per milliliter using cell supernatants as previously described (*69*, *70*).

Protein expression and purification

Genes encoding human apoferritin fusions, Fabs, Fcs, and IgGs were synthesized and cloned by GeneArt (Thermo Fisher Scientific) in the pcDNA3.4 expression vector and transiently expressed in HEK 293F cells. IgG1 and IgG4* versions of Fc were used, where IgG4* indicates the inclusion of the following mutations in the IgG4 Fc to ablate FcγR binding: S228P, F234A, L235A, G237A, and P238S (*45*). Cells were cultured at a density of 0.8×10^6 cells per ml and transfected with 50 μg of DNA per 200 ml of cells using FectoPRO (Polyplus Transfections, Strasbourg, France) as previously described (*40*). After 6 to 7 days of incubation with oscillation (Multitron-Pro shaker, Infors HT, 125-rpm oscillation, 37°C, 8% CO_2, and 70% humidity), cells were harvested by centrifugation at 5000 rpm for 20 min, and supernatants were filtered through a 0.22-μm Steritop filter (EMD Millipore). Fabs and IgGs were expressed by transiently cotransfecting 90 μg of heavy and light chain at a 2:1 ratio and purified using KappaSelect affinity and HiTrap Protein A HP columns, respectively (both GE Healthcare), eluted with 100 mM glycine (pH 2.2), and neutralized with 1 M tris-HCl (pH 9.0). IgG fractions were further purified by size exclusion chromatography (Superdex 200 Increase, GE Healthcare), and Fab fractions were further purified by cation exchange chromatography (MonoS, GE Healthcare). His-tagged WT RBD (BEI NR52309) and human and mouse Fc receptors (hFcγRI, hFcγRIIa, hFcγRIIb, hFcRn, mFcγRI, mFcγRIIb, mFcγRIV, and mFcRn) were purified using a HisTrap nickel–nitrilotriacetic acid column followed by size exclusion chromatography (Superdex 200 Increase column; both GE Healthcare) using 20 mM phosphate (pH 8.0) and 150 mM NaCl buffer.

Expression and purification of MBs

MBs were designed, expressed, and purified as previously described (*40*). Briefly, genes encoding scFab and scFc linked to human apoferritin light-chain monomers were synthesized and cloned by GeneArt (Thermo Fisher Scientific) into the pcDNA3.4 expression vector. MBs were expressed by transient transfection of 66 μg of plasmid (scFab-apoferritin: scFc-N-Ferr: scFab-C-Ferr at a 2:1:1 ratio for mono-specific MBs; or a 4:2:1:1 ratio of scFab1-apoferritin: scFc-N-Ferr: scFab2-C-Ferr: scFab3-C-Ferr for tri-specific MBs) into HEK 293F cells using FectoPRO (Polyplus Transfections). MBs were purified by affinity chromatography using a HiTrap Protein A HP column (GE Healthcare) and eluted with 20 mM tris (pH 8.0), 3 M $MgCl_2$, and 10% glycerol. Fractions were concentrated and further purified by gel filtration (Superose 6 10/300 GL column, GE Healthcare). For the tri-specific MB (298-52-80), an IgG1 or IgG4* scFc was used, where MB* indicates the use of an IgG4 with the FcγR binding mutations specified above (*45*). For in vivo studies, all IgGs and MBs were quality-controlled to ensure endotoxin concentrations below 3.5 EU/ml at a 1 mg/ml concentration of protein (*71*).

Statistical analysis

Statistical analyses were performed using Prism version 9.3.1 software (GraphPad Software Inc.). A $P < 0.005$ was considered statistically significant unless adjusted for multiple testing using the Bonferroni correction. Survival curves were compared using the Gehan-Breslow-Wilcoxon test, ADCP effector function data were compared by analysis of variance (ANOVA), and viral outgrowth data (not normally distributed) were compared using the Kruskal-

Wallis test. Data are shown as means ± SEM unless otherwise indicated.

Supplementary Materials

This PDF file includes:
Supplementary Materials and Methods
Figs. S1 to S10
Tables S1 to S3
References (*72*–*92*)

Other Supplementary Material for this manuscript includes the following:
Data file S1
MDAR Reproducibility Checklist

View/request a protocol for this paper from *Bio-protocol*.

REFERENCES AND NOTES

1. H. Ritchie, E. Mathieu, L. Rodés-Guirao, C. Appel, C. Giattino, E. Ortiz-Ospina, J. Hasell, B. Macdonald, D. Beltekian, M. Roser, *Coronavirus Pandemic (COVID-19)* (Our World in Data, 2020);https://ourworldindata.org/coronavirus.
2. D. S. Khoury, D. Cromer, A. Reynaldi, T. E. Schlub, A. K. Wheatley, J. A. Juno, K. Subbarao, S. J. Kent, J. A. Triccas, M. P. Davenport, Neutralizing antibody levels are highly predictive of immune protection from symptomatic SARS-CoV-2 infection. *Nat. Med.* **27**, 1205–1211 (2021).
3. V.-V. Edara, B. A. Pinsky, M. S. Suthar, L. Lai, M. E. Davis-Gardner, K. Floyd, M. W. Flowers, J. Wrammert, L. Hussaini, C. R. Ciric, S. Bechnak, K. Stephens, B. S. Graham, E. B. Mokhtari, P. Mudvari, E. Boritz, A. Creanga, A. Pegu, A. Derrien-Colemyn, A. R. Henry, M. Gagne, D. C. Douek, M. K. Sahoo, M. Sibai, D. Solis, R. J. Webby, T. Jeevan, T. P. Fabrizio, Infection and vaccine-induced neutralizing-antibody responses to the SARS-CoV-2 B.1.617 variants. *N. Engl. J. Med.* **385**, NEJMc2107799 (2021).
4. D. Planas, D. Veyer, A. Baidaliuk, I. Staropoli, F. Guivel-Benhassine, M. M. Rajah, C. Planchais, F. Porrot, N. Robillard, J. Puech, M. Prot, F. Gallais, P. Gantner, A. Velay, J. L. Guen, N. Kassis-Chikhani, D. Edriss, L. Belec, A. Seve, L. Courtellemont, H. Péré, L. Hocqueloux, S. Fafi-Kremer, T. Prazuck, H. Mouquet, T. Bruel, E. Simon-Lorière, F. A. Rey, O. Schwartz, Reduced sensitivity of SARS-CoV-2 variant Delta to antibody neutralization. *Nature* **596**, 276–280 (2021).
5. E. G. Levin, Y. Lustig, C. Cohen, R. Fluss, V. Indenbaum, S. Amit, R. Doolman, K. Asraf, E. Mendelson, A. Ziv, C. Rubin, L. Freedman, Y. Kreiss, G. Regev-Yochay, Waning immune humoral response to BNT162b2 covid-19 vaccine over 6 months. *N. Engl. J. Med.* **385**, NEJMoa2114583 (2021).
6. G. N. Sapkal, P. D. Yadav, R. R. Sahay, G. Deshpande, N. Gupta, D. A. Nyayanit, D. Y. Patil, A. M. Shete, S. Kumar, P. Abraham, S. Panda, B. Bhargava, Neutralization of Delta variant with sera of Covishield™ vaccinees and COVID-19-recovered vaccinated individuals. *J. Travel Med.* **28**, taab119 (2021).
7. P. Naaber, L. Tserel, K. Kangro, E. Sepp, V. Jürjenson, A. Adamson, L. Haljasmägi, A. P. Rumm, R. Maruste, J. Kärner, J. M. Gerhold, A. Planken, M. Ustav, K. Kisand, P. Peterson, Dynamics of antibody response to BNT162b2 vaccine after six months: A longitudinal prospective study. *Lancet Reg. Health Eur.* **10**, 100208 (2021).
8. V. Hall, S. Foulkes, F. Insalata, P. Kirwan, A. Saei, A. Atti, E. Wellington, J. Khawam, K. Munro, M. Cole, C. Tranquillini, A. Taylor-Kerr, N. Hettiarachchi, D. Calbraith, N. Sajedi, I. Milligan, Y. Themistocleous, D. Corrigan, L. Cromey, L. Price, S. Stewart, E. de Lacy, C. Norman, E. Linley, A. D. Otter, A. Semper, J. Hewson, S. D'Arcangelo, M. Chand, C. S. Brown, T. Brooks, J. Islam, A. Charlett, S. Hopkins; SIREN Study Group, Protection against SARS-CoV-2 after Covid-19 vaccination and previous infection. *N. Engl. J. Med.* **386**, 1207–1220 (2022).
9. N. Andrews, J. Stowe, F. Kirsebom, S. Toffa, T. Rickeard, E. Gallagher, C. Gower, M. Kall, N. Groves, A.-M. O'Connell, D. Simons, P. B. Blomquist, A. Zaidi, S. Nash, N. I. B. A. Aziz, S. Thelwall, G. Dabrera, R. Myers, G. Amirthalingam, S. Gharbia, J. C. Barrett, R. Elson, S. N. Ladhani, N. Ferguson, M. Zambon, C. N. J. Campbell, K. Brown, S. Hopkins, M. Chand, M. Ramsay, J. L. Bernal, Covid-19 vaccine effectiveness against the omicron (B.1.1.529) variant. *N. Engl. J. Med.* **386**, 1532–1546 (2022).
10. H. Chemaitelly, H. H. Ayoub, S. AlMukdad, P. Coyle, P. Tang, H. M. Yassine, H. A. Al-Khatib, M. K. Smatti, M. R. Hasan, Z. Al-Kanaani, E. Al-Kuwari, A. Jeremijenko, A. H. Kaleeckal, A. N. Latif, R. M. Shaik, H. F. Abdul-Rahim, G. K. Nasrallah, M. G. Al-Kuwari, A. A. Butt, H. E. Al-Romaihi, M. H. Al-Thani, A. Al-Khal, R. Bertollini, L. J. Abu-Raddad, Duration of mRNA vaccine protection against SARS-CoV-2 Omicron BA.1 and BA.2 subvariants in Qatar. *Nat. Commun.* **13**, 3082 (2022).
11. The IMpact-RSV Study Group, Palivizumab, a Humanized Respiratory Syncytial Virus Monoclonal Antibody, Reduces hospitalization from respiratory syncytial virus infection in high-risk infants. *Pediatrics* **102**, 531–537 (1998).
12. S. Mulangu, L. E. Dodd, R. T. Davey, O. T. Mbaya, M. Proschan, D. Mukadi, M. L. Manzo, D. Nzolo, A. T. Oloma, A. Ibanda, R. Ali, S. Coulibaly, A. C. Levine, R. Grais, J. Diaz, H. C. Lane, J.-J. Muyembe-Tamfum; PALM Writing Group, B. Sivahera, M. Camara, R. Kojan, R. Walker, B. Dighero-Kemp, H. Cao, P. Mukumbayi, P. Mbala-Kingebeni, S. Ahuka, S. Albert, T. Bonnett, I. Crozier, M. Duvenhage, C. Proffitt, M. Teitelbaum, T. Moench, J. Aboulhab, K. Barrett, K. Cahill, K. Cone, R. Eckes, L. Hensley, B. Herpin, E. Higgs, J. Ledgerwood, J. Pierson, M. Smolskis, Y. Sow, J. Tierney, S. Sivapalasingam, W. Holman, N. Gettinger, D. Vallée, J. Nordwall; PALM Consortium Study Team, A randomized, controlled trial of ebola virus disease therapeutics. *N. Engl. J. Med.* **381**, 2293–2303 (2019).
13. M. Dougan, A. Nirula, M. Azizad, B. Mocherla, R. L. Gottlieb, P. Chen, C. Hebert, R. Perry, J. Boscia, B. Heller, J. Morris, C. Crystal, A. Igbinadolor, G. Huhn, J. Cardona, I. Shawa, P. Kumar, A. C. Adams, J. V. Naarden, K. L. Custer, M. Durante, G. Oakley, A. E. Schade, T. R. Holzer, P. J. Ebert, R. E. Higgs, N. L. Kallewaard, J. Sabo, D. R. Patel, M. C. Dabora, P. Klekotka, L. Shen, D. M. Skovronsky; BLAZE-1 Investigators, Bamlanivimab plus etesevimab in mild or moderate Covid-19. *N. Engl. J. Med.* **385**, 1382–1392 (2021).
14. D. M. Weinreich, S. Sivapalasingam, T. Norton, S. Ali, H. Gao, R. Bhore, J. Xiao, A. T. Hooper, J. D. Hamilton, B. J. Musser, D. Rofail, M. Hussein, J. Im, D. Y. Atmodjo, C. Perry, C. Pan, A. Mahmood, R. Hosain, J. D. Davis, K. C. Turner, A. Baum, C. A. Kyratsous, Y. Kim, A. Cook, W. Kampman, L. Roque-Guerrero, G. Acloque, H. Aazami, K. Cannon, J. A. Simón-Campos, J. A. Bocchini, B. Kowal, A. T. DiCioccio, Y. Soo, G. P. Geba, N. Stahl, L. Lipsich, N. Braunstein, G. Herman, G. D. Yancopoulos; Trial Investigators, REGEN-COV Antibody Combination and Outcomes in Outpatients with Covid-19. *N. Engl. J. Med.* **385**, NEJMoa2108163 (2021).
15. M. Falcone, G. Tiseo, B. Valoriani, C. Barbieri, S. Occhineri, P. Mazzetti, M. L. Vatteroni, L. R. Suardi, N. Riccardi, M. Pistello, D. Tacconi, F. Menichetti, Efficacy of Bamlanivimab/Etesevimab and Casirivimab/Imdevimab in preventing progression to severe COVID-19 and role of variants of concern. *Infect. Dis. Ther.* **10**, 2479–2488 (2021).
16. U.S. Food and Drug Administration, *Coronavirus (COVID-19) Update: FDA Limits Use of Certain Monoclonal Antibodies to Treat COVID-19 due to the Omicron Variant* (U.S. Food and Drug Administration, 2022).
17. K. Westendorf, S. Žentelis, L. Wang, D. Foster, P. Vaillancourt, M. Wiggin, E. Lovett, R. van der Lee, J. Hendle, A. Pustilnik, J. M. Sauder, L. Kraft, Y. Hwang, R. W. Siegel, J. Chen, B. A. Heinz, R. E. Higgs, N. L. Kallewaard, K. Jepson, R. Goya, M. A. Smith, D. W. Collins, D. Pellacani, P. Xiang, V. de Puyraimond, M. Ricicova, L. Devorkin, C. Pritchard, A. O'Neill, K. Dalal, P. Panwar, H. Dhupar, F. A. Garces, C. A. Cohen, J. M. Dye, K. E. Huie, C. V. Badger, D. Kobasa, J. Audet, J. J. Freitas, S. Hassanali, I. Hughes, L. Munoz, H. C. Palma, B. Ramamurthy, R. W. Cross, T. W. Geisbert, V. Menachery, K. Lokugamage, V. Borisevich, I. Lanz, L. Anderson, P. Sipahimalani, K. S. Corbett, E. S. Yang, Y. Zhang, W. Shi, T. Zhou, M. Choe, J. Misasi, P. D. Kwong, N. J. Sullivan, B. S. Graham, T. L. Fernandez, C. L. Hansen, E. Falconer, J. R. Mascola, B. E. Jones, B. C. Barnhart, LY-CoV1404 (bebtelovimab) potently neutralizes SARS-CoV-2 variants. *Cell Rep.* **39**, 110812–110812 (2022).
18. U.S. Food and Drug Administration, *Coronavirus (COVID-19) Update: FDA Authorizes New Monoclonal Antibody for Treatment of COVID-19 that Retains Activity Against Omicron Variant* (U.S. Food and Drug Administration, 2022).
19. M. J. Levin, A. Ustianowski, S. D. Wit, O. Launay, M. Avila, A. Templeton, Y. Yuan, S. Seegobin, A. Ellery, D. J. Levinson, P. Ambery, R. H. Arends, R. Beavon, K. Dey, P. Garbes, E. J. Kelly, G. C. K. W. Koh, K. A. Near, K. W. Padilla, K. Psachoulia, A. Sharbaugh, K. Streicher, M. N. Pangalos, M. T. Esser; PROVENT Study Group, Intramuscular AZD7442 (Tixagevimab–Cilgavimab) for Prevention of Covid-19. *N. Engl. J. Med.* **386**, NEJMoa2116620 (2022).
20. U.S. Food and Drug Administration, *FDA Authorizes Revisions to Evusheld Dosing* (U.S. Food and Drug Administration, 2022).
21. U.S. Food and Drug Administration, *FDA Updates on Bebtelovimab* (U.S. Food and Drug Administration, 2022).
22. A. Z. Wec, D. Wrapp, A. S. Herbert, D. P. Maurer, D. Haslwanter, M. Sakharkar, R. K. Jangra, M. E. Dieterle, A. Lilov, D. Huang, L. V. Tse, N. V. Johnson, C.-L. Hsieh, N. Wang, J. H. Nett, E. Champney, I. Burnina, M. Brown, S. Lin, M. Sinclair, C. Johnson, S. Pudi, R. Bortz, A. S. Wirchnianski, E. Laudermilch, C. Florez, J. M. Fels, C. M. O'Brien, B. S. Graham, D. Nemazee, D. R. Burton, R. S. Baric, J. E. Voss, K. Chandran, J. M. Dye, J. S. McLellan, L. M. Walker, Broad neutralization of SARS-related viruses by human monoclonal antibodies. *Science* **369**, 731–736 (2020).
23. D. Pinto, M. M. Sauer, N. Czudnochowski, J. S. Low, M. A. Tortorici, M. P. Housley, J. Noack, A. C. Walls, J. E. Bowen, B. Guarino, L. E. Rosen, J. di Iulio, J. Jerak, H. Kaiser, S. Islam, S. Jaconi, N. Sprugasci, K. Culap, R. Abdelnabi, C. Foo, L. Coelmont, I. Bartha, S. Bianchi, C. Silacci-Fregni, J. Bassi, R. Marzi, E. Vetti, A. Cassotta, A. Ceschi, P. Ferrari, P. E. Cippà, O. Giannini, S. Ceruti, C. Garzoni, A. Riva, F. Benigni, E. Cameroni, L. Piccoli, M. S. Pizzuto, M. Smithey, D. Hong, A. Telenti, F. A. Lempp, J. Neyts, C. Havenar-Daughton, A. Lanzavecchia, F. Sallusto,

G. Snell, H. W. Virgin, M. Beltramello, D. Corti, D. Veesler, Broad betacoronavirus neutralization by a stem helix–Specific human antibody. *Science* **373**, 1109–1116 (2021).
24. D. Pinto, Y.-J. Park, M. Beltramello, A. C. Walls, M. A. Tortorici, S. Bianchi, S. Jaconi, K. Culap, F. Zatta, A. D. Marco, A. Peter, B. Guarino, R. Spreafico, E. Cameroni, J. B. Case, R. E. Chen, C. Havenar-Daughton, G. Snell, A. Telenti, H. W. Virgin, A. Lanzavecchia, M. S. Diamond, K. Fink, D. Veesler, D. Corti, Cross-neutralization of SARS-CoV-2 by a human monoclonal SARS-CoV antibody. *Nature* **583**, 290–295 (2020).
25. P. Wang, R. G. Casner, M. S. Nair, J. Yu, Y. Guo, M. Wang, J. F.-W. Chan, G. Cerutti, S. Iketani, L. Liu, Z. Sheng, Z. Chen, K.-Y. Yuen, P. D. Kwong, Y. Huang, L. Shapiro, D. D. Ho, A monoclonal antibody that neutralizes SARS-CoV-2 variants, SARS-CoV, and other sarbecoviruses. *Emerg. Microbes. Infect.* **11**, 147–157 (2021).
26. T. N. Starr, N. Czudnochowski, Z. Liu, F. Zatta, Y.-J. Park, A. Addetia, D. Pinto, M. Beltramello, P. Hernandez, A. J. Greaney, R. Marzi, W. G. Glass, I. Zhang, A. S. Dingens, J. E. Bowen, M. A. Tortorici, A. C. Walls, J. A. Wojcechowskyj, A. D. Marco, L. E. Rosen, J. Zhou, M. Montiel-Ruiz, H. Kaiser, J. R. Dillen, H. Tucker, J. Bassi, C. Silacci-Fregni, M. P. Housley, J. di Iulio, G. Lombardo, M. Agostini, N. Sprugasci, K. Culap, S. Jaconi, M. Meury, E. D. Jr, R. Abdelnabi, S.-Y. C. Foo, E. Cameroni, S. Stumpf, T. I. Croll, J. C. Nix, C. Havenar-Daughton, L. Piccoli, F. Benigni, J. Neyts, A. Telenti, F. A. Lempp, M. S. Pizzuto, J. D. Chodera, C. M. Hebner, H. W. Virgin, S. P. J. Whelan, D. Veesler, D. Corti, J. D. Bloom, G. Snell, SARS-CoV-2 RBD antibodies that maximize breadth and resistance to escape. *Nature* **597**, 97–102 (2021).
27. P. Zhou, M. Yuan, G. Song, N. Beutler, N. Shaabani, D. Huang, W. He, X. Zhu, S. Callaghan, P. Yong, F. Anzanello, L. Peng, J. Ricketts, M. Parren, E. Garcia, S. A. Rawlings, D. M. Smith, D. Nemazee, J. R. Teijaro, T. F. Rogers, I. A. Wilson, D. R. Burton, R. Andrabi, A human antibody reveals a conserved site on beta-coronavirus spike proteins and confers protection against SARS-CoV-2 infection. *Sci. Transl. Med.* **14**, eabi9215 (2022).
28. Y. Wang, M. Liu, Y. Shen, Y. Ma, X. Li, Y. Zhang, M. Liu, X.-L. Yang, J. Chen, R. Yan, D. Luan, Y. Wang, Y. Chen, Q. Wang, H. Lin, Y. Li, K. Wu, T. Zhu, J. Zhao, H. Lu, Y. Wen, S. Jiang, F. Wu, Q. Zhou, Z.-L. Shi, J. Huang, Novel sarbecovirus bispecific neutralizing antibodies with exceptional breadth and potency against currently circulating SARS-CoV-2 variants and sarbecoviruses. *Cell Discov.* **8**, 36 (2022).
29. E. Cameroni, J. E. Bowen, L. E. Rosen, C. Saliba, S. K. Zepeda, K. Culap, D. Pinto, L. A. VanBlargan, A. D. Marco, J. di Iulio, F. Zatta, H. Kaiser, J. Noack, N. Farhat, N. Czudnochowski, C. Havenar-Daughton, K. R. Sprouse, J. R. Dillen, A. E. Powell, A. Chen, C. Maher, L. Yin, D. Sun, L. Soriaga, J. Bassi, C. Silacci-Fregni, C. Gustafsson, N. M. Franko, J. Logue, N. T. Iqbal, I. Mazzitelli, J. Geffner, R. Grifantini, H. Chu, A. Gori, A. Riva, O. Giannini, A. Ceschi, P. Ferrari, P. E. Cippà, A. Franzetti-Pellanda, C. Garzoni, P. J. Halfmann, Y. Kawaoka, C. Hebner, L. A. Purcell, L. Piccoli, M. S. Pizzuto, A. C. Walls, M. S. Diamond, A. Telenti, H. W. Virgin, A. Lanzavecchia, G. Snell, D. Veesler, D. Corti, Broadly neutralizing antibodies overcome SARS-CoV-2 Omicron antigenic shift. *Nature* **602**, 664–670 (2022).
30. J. Icenogle, H. Shiwen, G. Duke, S. Gilbert, R. Rueckert, J. Anderegg, Neutralization of poliovirus by a monoclonal antibody: Kinetics and stoichiometry. *Virology* **127**, 412–425 (1983).
31. L. A. Cavacini, C. L. Emes, J. Power, M. Duval, M. R. Posner, Effect of antibody valency on interaction with cell-surface expressed HIV-1 and viral neutralization. *J. Immunol.* **152**, 2538–2545 (1994).
32. H. Wu, D. S. Pfarr, Y. Tang, L.-L. An, N. K. Patel, J. D. Watkins, W. D. Huse, P. A. Kiener, J. F. Young, Ultra-potent antibodies against respiratory syncytial virus: Effects of binding kinetics and binding valence on viral neutralization. *J. Mol. Biol.* **350**, 126–144 (2005).
33. S. C. Oostindie, G. A. Lazar, J. Schuurman, P. W. H. I. Parren, Avidity in antibody effector functions and biotherapeutic drug design. *Nat. Rev. Drug Discov.* **21**, 715–735 (2022).
34. Z. Ku, X. Xie, P. R. Hinton, X. Liu, X. Ye, A. E. Muruato, D. C. Ng, S. Biswas, J. Zou, Y. Liu, D. Pandya, V. D. Menachery, S. Rahman, Y.-A. Cao, H. Deng, W. Xiong, K. B. Carlin, J. Liu, H. Su, E. J. Haanes, B. A. Keyt, N. Zhang, S. F. Carroll, P.-Y. Shi, Z. An, Nasal delivery of an IgM offers broad protection from SARS-CoV-2 variants. *Nature* **595**, 718–723 (2021).
35. R. Divine, H. V. Dang, G. Ueda, J. A. Fallas, I. Vulovic, W. Sheffler, S. Saini, Y. T. Zhao, I. X. Raj, P. A. Morawski, M. F. Jennewein, L. J. Homad, Y.-H. Wan, M. R. Tooley, F. Seeger, A. Etemadi, M. L. Fahning, J. Lazarovits, A. Roederer, A. C. Walls, L. Stewart, M. Mazloomi, N. P. King, D. J. Campbell, A. T. McGuire, L. Stamatatos, H. Ruohola-Baker, J. Mathieu, D. Veesler, D. Baker, Designed proteins assemble antibodies into modular nanocages. *Science* **372**, eabd9994 (2021).
36. Y. Han, Z. Yang, H. Hu, H. Zhang, L. Chen, K. Li, L. Kong, Q. Wang, B. Liu, M. Wang, J. Lin, P. R. Chen, Covalently engineered protein minibinders with enhanced neutralization efficacy against escaping SARS-CoV-2 variants. *J. Am. Chem. Soc.* **144**, 5702–5707 (2022).
37. S. C. Oostindie, H. J. van der Horst, L. P. Kil, K. Strumane, M. B. Overdijk, E. N. van den Brink, J. H. N. van den Brakel, H. J. Rademaker, B. van Kessel, J. van den Noort, M. E. D. Chamuleau, T. Mutis, M. A. Lindorfer, R. P. Taylor, J. Schuurman, P. W. H. I. Parren, F. J. Beurskens, E. C. W. Breij, DuoHexaBody-CD37®, a novel biparatopic CD37 antibody with enhanced Fc-mediated hexamerization as a potential therapy for B-cell malignancies. *Blood Cancer J.* **10**, 30 (2020).
38. E. Rowell, H. Kinkead, E. Torretti, B. Becklund, F. Sulzmaier, W. Crago, K. Jones, J. Timmer, Q. Deveraux, B. Eckelman, A. Heidt, 856 INBRX-106: a novel hexavalent anti-OX40 agonist for the treatment of solid tumors. *J. Immunother. Cancer* **9**, A897–A897 (2021).
39. B. T. Wang, T. Kothambawala, L. Wang, T. J. Matthew, S. E. Calhoun, A. K. Saini, M. F. Kotturi, G. Hernandez, E. W. Humke, M. S. Peterson, A. M. Sinclair, B. A. Keyt, Multimeric anti-DR5 IgM agonist antibody IGM-8444 is a potent inducer of cancer cell Apoptosis and synergizes with chemotherapy and BCL-2 inhibitor ABT-199. *Mol. Cancer Ther.* **20**, 2483–2494 (2021).
40. E. Rujas, I. Kucharska, Y. Z. Tan, S. Benlekbir, H. Cui, T. Zhao, G. A. Wasney, P. Budylowski, F. Guvenc, J. C. Newton, T. Sicard, A. Semesi, K. Muthuraman, A. Nouanesengsy, C. B. Aschner, K. Prieto, S. A. Bueler, S. Youssef, S. Liao-Chan, J. Glanville, N. Christie-Holmes, S. Mubareka, S. D. Gray-Owen, J. L. Rubinstein, B. Treanor, J.-P. Julien, Multivalency transforms SARS-CoV-2 antibodies into ultrapotent neutralizers. *Nat. Commun.* **12**, 3661 (2021).
41. E. Rujas, H. Cui, J. Burnie, C. B. Aschner, T. Zhao, S. Insausti, K. Muthuraman, A. Semesi, J. Ophel, J. L. Nieva, M. S. Seaman, C. Guzzo, B. Treanor, J.-P. Julien, Engineering pan–HIV-1 neutralization potency through multispecific antibody avidity. *Proc. Natl. Acad. Sci. U.S.A.* **119**, e2112887119 (2022).
42. L. Liu, S. Iketani, Y. Guo, J. F.-W. Chan, M. Wang, L. Liu, Y. Luo, H. Chu, Y. Huang, M. S. Nair, J. Yu, K. K.-H. Chik, T. T.-T. Yuen, C. Yoon; K. K.-W. To, H. Chen, M. T. Yin, M. E. Sobieszczyk, Y. Huang, H. H. Wang, Z. Sheng, K.-Y. Yuen, D. D. Ho, Striking antibody evasion manifested by the Omicron variant of SARS-CoV-2. *Nature* **602**, 676–681 (2022).
43. E. Takashita, N. Kinoshita, S. Yamayoshi, Y. Sakai-Tagawa, S. Fujisaki, M. Ito, K. Iwatsuki-Horimoto, S. Chiba, P. Halfmann, H. Nagai, M. Saito, E. Adachi, D. Sullivan, A. Pekosz, S. Watanabe, K. Maeda, M. Imai, H. Yotsuyanagi, H. Mitsuya, N. Ohmagari, M. Takeda, H. Hasegawa, Y. Kawaoka, Efficacy of antibodies and antiviral drugs against covid-19 Omicron variant. *N. Engl. J. Med.* **386**, 995–998 (2022).
44. T. Tada, H. Zhou, B. M. Dcosta, M. I. Samanovic, V. Chivukula, R. S. Herati, S. R. Hubbard, M. J. Mulligan, N. R. Landau, Increased resistance of SARS-CoV-2 Omicron variant to neutralization by vaccine-elicited and therapeutic antibodies. *EBioMedicine* **78**, 103944 (2022).
45. S. Tam, S. McCarthy, A. Armstrong, S. Somani, S.-J. Wu, X. Liu, A. Gervais, R. Ernst, D. Saro, R. Decker, J. Luo, G. Gilliland, M. Chiu, B. Scallon, Functional, biophysical, and structural characterization of human IgG1 and IgG4 Fc variants with ablated immune functionality. *Antibodies (Basel)* **6**, 12 (2017).
46. A. Banerjee, J. A. Nasir, P. Budylowski, L. Yip, P. Aftanas, N. Christie, A. Ghalami, K. Baid, A. R. Raphenya, J. A. Hirota, M. S. Miller, A. J. McGeer, M. Ostrowski, R. A. Kozak, A. G. McArthur, K. Mossman, S. Mubareka, Isolation, sequence, infectivity, and replication kinetics of severe acute respiratory syndrome coronavirus 2. *Emerg. Infect. Dis.* **26**, 2054–2063 (2020).
47. D. Li, G. D. Sempowski, K. O. Saunders, P. Acharya, B. F. Haynes, SARS-CoV-2 neutralizing antibodies for COVID-19 prevention and treatment. *Annu. Rev. Med.* **73**, 1–16 (2021).
48. L. Liu, P. Wang, M. S. Nair, J. Yu, M. Rapp, Q. Wang, Y. Luo, J. F. W. Chan, V. Sahi, A. Figueroa, X. V. Guo, G. Cerutti, J. Bimela, J. Gorman, T. Zhou, Z. Chen, K.-Y. Yuen, P. D. Kwong, J. G. Sodroski, M. T. Yin, Z. Sheng, Y. Huang, L. Shapiro, D. D. Ho, Potent neutralizing antibodies against multiple epitopes on SARS-CoV-2 spike. *Nature* **584**, 450–456 (2020).
49. L. Liu, S. Iketani, Y. Guo, R. G. Casner, E. R. Reddem, M. S. Nair, J. Yu, J. F.-W. Chan, M. Wang, G. Cerutti, Z. Li, N. C. Morano, C. D. Castagna, L. Corredor, H. Chu, S. Yuan, V. K.-M. Poon, C. C.-S. Chan, Z. Chen, Y. Luo, M. Cunningham, A. Chavez, M. T. Yin, D. S. Perlin, M. Tsuji, K.-Y. Yuen, P. D. Kwong, Z. Sheng, Y. Huang, L. Shapiro, D. D. Ho, An antibody class with a common CDRH3 motif broadly neutralizes sarbecoviruses. *Sci. Transl. Med.* **14**, eabn6859 (2022).
50. D. M. Weinreich, S. Sivapalasingam, T. Norton, S. Ali, H. Gao, R. Bhore, B. J. Musser, Y. Soo, D. Rofail, J. Im, C. Perry, C. Pan, R. Hosain, A. Mahmood, J. D. Davis, K. C. Turner, A. T. Hooper, J. D. Hamilton, A. Baum, C. A. Kyratsous, Y. Kim, A. Cook, W. Kampman, A. Kohli, Y. Sachdeva, X. Graber, B. Kowal, T. DiCioccio, N. Stahl, L. Lipsich, N. Braunstein, G. Herman, G. D. Yancopoulos, T. Investigators, REGN-COV2, a neutralizing antibody cocktail, in outpatients with covid-19. *N. Engl. J. Med.* **384**, 238–251 (2020).
51. L. A. VanBlargan, J. M. Errico, P. J. Halfmann, S. J. Zost, J. E. Crowe Jr., L. A. Purcell, Y. Kawaoka, D. Corti, D. H. Fremont, M. S. Diamond, An infectious SARS-CoV-2 B.1.1.529 Omicron virus escapes neutralization by therapeutic monoclonal antibodies. *Nat. Med.* **28**, 490–495 (2022).
52. G. Cerutti, M. Rapp, Y. Guo, F. Bahna, J. Bimela, E. R. Reddem, J. Yu, P. Wang, L. Liu, Y. Huang, D. D. Ho, P. D. Kwong, Z. Sheng, L. Shapiro, Structural basis for accommodation of emerging B.1.351 and B.1.1.7 variants by two potent SARS-CoV-2 neutralizing antibodies. *Structure* **29**, 655–663.e4 (2021).
53. W. Li, Y. Chen, J. Prévost, I. Ullah, M. Lu, S. Y. Gong, A. Tauzin, R. Gasser, D. Vézina, S. P. Anand, G. Goyette, D. Chaterjee, S. Ding, W. D. Tolbert, M. W. Grunst, Y. Bo, S. Zhang, J. Richard, F. Zhou, R. K. Huang, L. Esser, A. Zeher, M. Côté, P. Kumar, J. Sodroski, D. Xia, P. D. Uchil, M. Pazgier, A. Finzi, W. Mothes, Structural basis and mode of action for two broadly neutralizing antibodies against SARS-CoV-2 emerging variants of concern. *Cell Rep.* **38**, 110210 (2022).

54. Q. Wang, S. Iketani, Z. Li, L. Liu, Y. Guo, Y. Huang, A. D. Bowen, M. Liu, M. Wang, J. Yu, R. Valdez, A. S. Lauring, Z. Sheng, H. H. Wang, A. Gordon, L. Liu, D. D. Ho, Alarming antibody evasion properties of rising SARS-CoV-2 BQ and XBB subvariants. *Cell* **186**, 279–286.e8 (2023).
55. G. Ueda, A. Antanasijevic, J. A. Fallas, W. Sheffler, J. Copps, D. Ellis, G. B. Hutchinson, A. Moyer, A. Yasmeen, Y. Tsybovsky, Y.-J. Park, M. J. Bick, B. Sankaran, R. A. Gillespie, P. J. Brouwer, P. H. Zwart, D. Veesler, M. Kanekiyo, B. S. Graham, R. W. Sanders, J. P. Moore, P. J. Klasse, A. B. Ward, N. P. King, D. Baker, Tailored design of protein nanoparticle scaffolds for multivalent presentation of viral glycoprotein antigens. *Elife* **9**, e57659 (2020).
56. P. J. M. Brouwer, A. Antanasijevic, Z. Berndsen, A. Yasmeen, B. Fiala, T. P. L. Bijl, I. Bontjer, J. B. Bale, W. Sheffler, J. D. Allen, A. Schorcht, J. A. Burger, M. Camacho, D. Ellis, C. A. Cottrell, A.-J. Behrens, M. Catalano, I. del Moral-Sánchez, T. J. Ketas, C. LaBranche, M. J. van Gils, K. Sliepen, L. J. Stewart, M. Crispin, D. C. Montefiori, D. Baker, J. P. Moore, P. J. Klasse, A. B. Ward, N. P. King, R. W. Sanders, Enhancing and shaping the immunogenicity of native-like HIV-1 envelope trimers with a two-component protein nanoparticle. *Nat. Commun.* **10**, 4272 (2019).
57. S. Boyoglu-Barnum, D. Ellis, R. A. Gillespie, G. B. Hutchinson, Y.-J. Park, S. M. Moin, O. J. Acton, R. Ravichandran, M. Murphy, D. Pettie, N. Matheson, L. Carter, A. Creanga, M. J. Watson, S. Kephart, S. Ataca, J. R. Vaile, G. Ueda, M. C. Crank, L. Stewart, K. K. Lee, M. Guttman, D. Baker, J. R. Mascola, D. Veesler, B. S. Graham, N. P. King, M. Kanekiyo, Quadrivalent influenza nanoparticle vaccines induce broad protection. *Nature* **592**, 623–628 (2021).
58. A. Antanasijevic, G. Ueda, P. J. M. Brouwer, J. Copps, D. Huang, J. D. Allen, C. A. Cottrell, A. Yasmeen, L. M. Sewall, I. Bontjer, T. J. Ketas, H. L. Turner, Z. T. Berndsen, D. C. Montefiori, P. J. Klasse, M. Crispin, D. Nemazee, J. P. Moore, R. W. Sanders, N. P. King, D. Baker, A. B. Ward, Structural and functional evaluation of de novo-designed, two-component nanoparticle carriers for HIV Env trimer immunogens. *PLOS Pathog.* **16**, e1008665 (2020).
59. S. Shi, Biologics: An update and challenge of their pharmacokinetics. *Curr. Drug Metab.* **15**, 271–290 (2014).
60. B. J. Booth, B. Ramakrishnan, K. Narayan, A. M. Wollacott, G. J. Babcock, Z. Shriver, K. Viswanathan, Extending human IgG half-life using structure-guided design. *MAbs* **10**, 1098–1110 (2018).
61. A. Schäfer, F. Muecksch, J. C. C. Lorenzi, S. R. Leist, M. Cipolla, S. Bournazos, F. Schmidt, R. M. Maison, A. Gazumyan, D. R. Martinez, R. S. Baric, D. F. Robbiani, T. Hatziioannou, J. V. Ravetch, P. D. Bieniasz, R. A. Bowen, M. C. Nussenzweig, T. P. Sheahan, Antibody potency, effector function, and combinations in protection and therapy for SARS-CoV-2 infection in vivo. *J. Exp. Med.* **218**, e20201993 (2021).
62. E. S. Winkler, P. Gilchuk, J. Yu, A. L. Bailey, R. E. Chen, Z. Chong, S. J. Zost, H. Jang, Y. Huang, J. D. Allen, J. B. Case, R. E. Sutton, R. H. Carnahan, T. L. Darling, A. C. M. Boon, M. Mack, R. D. Head, T. M. Ross, J. E. Crowe, M. S. Diamond, Human neutralizing antibodies against SARS-CoV-2 require intact Fc effector functions for optimal therapeutic protection. *Cell* **184**, 1804–1820.e16 (2021).
63. C. E. Z. Chan, S. G. K. Seah, D. H. Chye, S. Massey, M. Torres, A. P. C. Lim, S. K. K. Wong, J. J. Y. Neo, P. S. Wong, J. H. Lim, G. S. L. Loh, D. Wang, J. D. Boyd-Kirkup, S. Guan, D. Thakkar, G. H. Teo, K. Purushotorman, P. E. Hutchinson, B. E. Young, J. G. Low, P. A. MacAry, H. Hentze, V. S. Prativadibhayankara, K. Ethirajulu, J. E. Comer, C.-T. K. Tseng, A. D. T. Barrett, P. J. Ingram, T. Brasel, B. J. Hanson, The Fc-mediated effector functions of a potent SARS-CoV-2 neutralizing antibody, SC31, isolated from an early convalescent COVID-19 patient, are essential for the optimal therapeutic efficacy of the antibody. *PLOS ONE* **16**, e0253487 (2021).
64. I. Ullah, J. Prévost, M. S. Ladinsky, H. Stone, M. Lu, S. P. Anand, G. Beaudoin-Bussières, K. Symmes, M. Benlarbi, S. Ding, R. Gasser, C. Fink, Y. Chen, A. Tauzin, G. Goyette, C. Bourassa, H. Medjahed, M. Mack, K. Chung, C. B. Wilen, G. A. Dekaban, J. D. Dikeakos, E. A. Bruce, D. E. Kaufmann, L. Stamatatos, A. T. McGuire, J. Richard, M. Pazgier, P. J. Bjorkman, W. Mothes, A. Finzi, P. Kumar, P. D. Uchil, Live imaging of SARS-CoV-2 infection in mice reveals that neutralizing antibodies require Fc function for optimal efficacy. *Immunity* **54**, 2143–2158.e15 (2021).
65. V. Dussupt, R. S. Sankhala, L. Mendez-Rivera, S. M. Townsley, F. Schmidt, L. Wieczorek, K. G. Lal, G. C. Donofrio, U. Tran, N. D. Jackson, W. I. Zaky, M. Zemil, S. R. Tritsch, W.-H. Chen, E. J. Martinez, A. Ahmed, M. Choe, W. C. Chang, A. Hajduczki, N. Jian, C. E. Peterson, P. A. Rees, M. Rutkowska, B. M. Slike, C. N. Selverian, I. Swafford, I.-T. Teng, P. V. Thomas, T. Zhou, C. J. Smith, J. R. Currier, P. D. Kwong, M. Rolland, E. Davidson, B. J. Doranz, C. N. Mores, T. Hatziioannou, W. W. Reiley, P. D. Bieniasz, D. Paquin-Proulx, G. D. Gromowski, V. R. Polonis, N. L. Michael, K. Modjarrad, M. G. Joyce, S. J. Krebs, Low-dose in vivo protection and neutralization across SARS-CoV-2 variants by monoclonal antibody combinations. *Nat. Immunol.* **22**, 1503–1514 (2021).
66. M. Sahin, M. M. Remy, B. Fallet, R. Sommerstein, M. Florova, A. Langner, K. Klausz, T. Straub, M. Kreutzfeldt, I. Wagner, C. T. Schmidt, P. Malinge, G. Magistrelli, S. Izui, H. Pircher, J. S. Verbeek, D. Merkler, M. Peipp, D. D. Pinschewer, Antibody bivalency improves antiviral efficacy by inhibiting virion release independently of Fc gamma receptors. *Cell Rep.* **38**, 110303 (2022).
67. S. E. Hufton, P. Risley, C. R. Ball, D. Major, O. G. Engelhardt, S. Poole, The breadth of cross sub-type neutralisation activity of a single domain antibody to influenza hemagglutinin can be increased by antibody valency. *PLOS ONE* **9**, e103294 (2014).
68. P. J. Klasse, Neutralization of virus infectivity by antibodies: Old problems in new perspectives. *Adv. Biol.* **2014**, 157895 (2014).
69. M. A. Hamilton, R. C. Russo, R. V. Thurston, Trimmed Spearman-Karber method for estimating median lethal concentrations in toxicity bioassays. *Environ. Sci. Technol.* **11**, 714–719 (1977).
70. A. Banerjee, D. Falzarano, N. Rapin, J. Lew, V. Misra, Interferon regulatory factor 3-mediated signaling limits Middle-East respiratory syndrome (MERS) coronavirus propagation in cells from an insectivorous bat. *Viruses* **11**, 152 (2019).
71. U.S. Food and Drug Administration, *Bacterial Endotoxins/Pyrogens Technical Guidelines* (U.S. Food and Drug Administration, 1985).
72. C. R. Marr, S. Benlekbir, J. L. Rubinstein, Fabrication of carbon films with ~500nm holes for cryo-EM with a direct detector device. *J. Struct. Biol.* **185**, 42–47 (2014).
73. A. Punjani, J. L. Rubinstein, D. J. Fleet, M. A. Brubaker, cryoSPARC: algorithms for rapid unsupervised cryo-EM structure determination. *Nat. Methods* **14**, 290–296 (2017).
74. A. Punjani, H. Zhang, D. J. Fleet, Non-uniform refinement: Adaptive regularization improves single-particle cryo-EM reconstruction. *Nat. Methods* **17**, 1214–1221 (2020).
75. Z. Wang, C. Li, M. Ellenburg, E. Soistman, J. Ruble, B. Wright, J. X. Ho, D. C. Carter, Structure of human ferritin L chain. *Acta Crystallogr. Sect. D Biol. Crystallogr.* **62**, 800–806 (2006).
76. Y. Z. Tan, J. L. Rubinstein, Through-grid wicking enables high-speed cryoEM specimen preparation. *Acta Crystallogr. D Struct. Biol.* **76**, 1092–1103 (2020).
77. C. Orlandi, D. Deredge, K. Ray, N. Gohain, W. Tolbert, A. L. DeVico, P. Wintrode, M. Pazgier, G. K. Lewis, Antigen-induced allosteric changes in a human IgG1 Fc increase low-affinity Fcγ receptor binding. *Structure* **28**, 516–527.e5 (2020).
78. E. F. Pettersen, T. D. Goddard, C. C. Huang, G. S. Couch, D. M. Greenblatt, E. C. Meng, T. E. Ferrin, UCSF Chimera—A visualization system for exploratory research and analysis. *J. Comput. Chem.* **25**, 1605–1612 (2004).
79. Schrodinger, *The PyMOL Molecular Graphics System* (2015).
80. T. D. Goddard, C. C. Huang, E. C. Meng, E. F. Pettersen, G. S. Couch, J. H. Morris, T. E. Ferrin, UCSF ChimeraX: Meeting modern challenges in visualization and analysis. *Protein Sci.* 27, 14–25 (2018).
81. K. H. D. Crawford, R. Eguia, A. S. Dingens, A. N. Loes, K. D. Malone, C. R. Wolf, H. Y. Chu, M. A. Tortorici, D. Veesler, M. Murphy, D. Pettie, N. P. King, A. B. Balazs, J. D. Bloom, Protocol and reagents for pseudotyping lentiviral particles with SARS-CoV-2 spike protein for neutralization assays. *Viruses* **12**, 513 (2020).
82. N. Wang, Y. Sun, R. Feng, Y. Wang, Y. Guo, L. Zhang, Y.-Q. Deng, L. Wang, Z. Cui, L. Cao, Y.-J. Zhang, W. Li, F.-C. Zhu, C.-F. Qin, X. Wang, Structure-based development of human antibody cocktails against SARS-CoV-2. *Cell Res.* **31**, 101–103 (2020).
83. V. M. Corman, O. Landt, M. Kaiser, R. Molenkamp, A. Meijer, D. K. Chu, T. Bleicker, S. Brünink, J. Schneider, M. L. Schmidt, D. G. Mulders, B. L. Haagmans, B. van der Veer, S. van den Brink, L. Wijsman, G. Goderski, J.-L. Romette, J. Ellis, M. Zambon, M. Peiris, H. Goossens, C. Reusken, M. P. Koopmans, C. Drosten, Detection of 2019 novel coronavirus (2019-nCoV) by real-time RT-PCR. *Euro Surveill.* **25**, 2000045 (2020).
84. W. Kabsch, XDS. *Acta. Crystallogr. D Biol. Crystallogr.* **66**, 125–132 (2010).
85. Bruker AXS Inc, *X-Ray Data Preparation and Reciprocal Space Exploration Program* (Bruker AXS Inc, 2014).
86. A. J. McCoy, R. W. Grosse-Kunstleve, P. D. Adams, M. D. Winn, L. C. Storoni, R. J. Read, Phaser crystallographic software. *J. Appl. Crystallogr.* **40**, 658–674 (2007).
87. J. Leem, J. Dunbar, G. Georges, J. Shi, C. M. Deane, ABodyBuilder: Automated antibody structure prediction with data–Driven accuracy estimation. *MAbs* **8**, 1259–1268 (2016).
88. H. Liu, M. Yuan, D. Huang, S. Bangaru, F. Zhao, C.-C. D. Lee, L. Peng, S. Barman, X. Zhu, D. Nemazee, D. R. Burton, M. J. van Gils, R. W. Sanders, H.-C. Kornau, S. M. Reincke, H. Prüss, J. Kreye, N. C. Wu, A. B. Ward, I. A. Wilson, A combination of cross-neutralizing antibodies synergizes to prevent SARS-CoV-2 and SARS-CoV pseudovirus infection. *Cell Host Microbe* **29**, 806–818.e6 (2021).
89. P. D. Adams, P. V. Afonine, G. Bunkóczi, V. B. Chen, I. W. Davis, N. Echols, J. J. Headd, L.-W. Hung, G. J. Kapral, R. W. Grosse-Kunstleve, A. J. McCoy, N. W. Moriarty, R. Oeffner, R. J. Read, D. C. Richardson, J. S. Richardson, T. C. Terwilliger, P. H. Zwart, PHENIX: A comprehensive Python-based system for macromolecular structure solution. *Acta Crystallogr. D Biol. Crystallogr.* **66**, 213–221 (2010).
90. P. Emsley, B. Lohkamp, W. G. Scott, K. Cowtan, Features and development of Coot. *Acta Crystallogr. D Biol. Crystallogr.* **66**, 486–501 (2010).
91. A. Morin, B. Eisenbraun, J. Key, P. C. Sanschagrin, M. A. Timony, M. Ottaviano, P. Sliz, Collaboration gets the most out of software. *eLife* **2**, e01456 (2013).

92. E. Krissinel, K. Henrick, Inference of macromolecular assemblies from crystalline state. *J. Mol. Biol.* **372**, 774–797 (2007).

Acknowledgments: We thank A. Banerjee and K. Mossman for contributions to the initial isolation of SARS-CoV-2 (SARS-CoV.2/SB-2-P4-PB Clone1); C. Siska for work on the polyreactivity assays; F. Krammer for providing the WT spike plasmid; D.R. Burton for providing the Omicron BA.1 spike plasmid; J. D. Bloom and A. C. Gingras for 293 T-ACE2 cells and reagents to make SARS-CoV-2 PsV; and S. Benlekbir for advice regarding cryo-EM data collection and specimen preparation. The following reagent was produced under HHSN272201400008C and obtained through BEI Resources, NIAID, NIH: Vector pCAGGS Containing the SARS-Related Coronavirus 2, Wuhan-Hu-1 Spike Glycoprotein Gene, NR-52310. Omicron BA.2 (NR-56512) used for this study was also sourced from BEI Resources, NIAID, NIH. **Funding:** This work was supported by Natural Sciences and Engineering Research Council of Canada discovery grant 6280100058 (to J.-P.J.), operating grant PJ4-169662 from the Canadian Institutes of Health Research (CIHR; to B.T. and J.-P.J.), COVID-19 Research Fund C-094-2424972-JULIEN (to J.-P.J.) from the Province of Ontario Ministry of Colleges and Universities, the Bill and Melinda Gates Foundation INV-023398 (to J.-P.J.), and the Hospital for Sick Children Foundation. This research was also supported by Hospital for Sick Children Restracomp Postdoctoral Fellowships (to C.B.A. and I.K.), an Ontario Graduate Scholarship (OGS; to K.M.), a Banting Postdoctoral Fellowship (to C.B.A.), the CIFAR Azrieli Global Scholar program (to J.-P.J.), the Ontario Early Researcher Awards program (to J.-P.J.), and the Canada Research Chairs program (to J.L.R., B.T., and J.-P.J.). Cryo-EM data were collected at the Toronto High-Resolution High-Throughput cryo-EM facility, and biophysical data were collected at the Structural and Biophysical Core Facility, both supported by the Canada Foundation for Innovation and Ontario Research Fund. X-ray diffraction experiments were performed at GM/CA@APS, which has been funded in whole or in part with federal funds from the National Cancer Institute (ACB-12002) and the National Institute of General Medical Sciences (AGM-12006). The EIGER 16M detector at GM/CA-XSD was funded by NIH grant S10 OD012289. This research used resources of the Advanced Photon Source, a U.S. Department of Energy (DOE) Office of Science user facility operated for the U.S. DOE Office of Science by Argonne National Laboratory under contract DE-AC02-06CH11357. **Author contributions:** C.B.A., K.M., A.J., and J.-P.J. conceived the research and designed the experiments. C.B.A., K.M., I.K., H.C., K.P., M.S.N., M.W., Y.H., B.P., J.L., and A.S. performed experimental work. C.B.A. executed and analyzed all in vivo and flow cytometry experiments. K.M. executed and analyzed biolayer interferometry, pseudo-virus neutralization, and x-ray crystallography experiments. I.K. performed and analyzed cryo-EM experiments. H.C. and K.P. provided experimental support for protein production and purification. M.S.N., M.W., and Y.H. performed authentic virus neutralization. B.P. and J.L. provided in vitro support for in vivo experiments. A.S. performed RT-qPCR. N.C.-H., R.K., and S.M. provided critical reagents. N.C.-H., R.K., S.M., and E.R. provided critical expertise. C.B.A., K.M., I.K., M.S.N., M.W., Y.H., J.L.R., B.T., D.D.H., A.J., and J.-P.J. analyzed the data. C.B.A., K.M., I.K., E.R., A.J., and J.-P.J. wrote the manuscript with input from all authors. **Competing interests:** The Hospital for Sick Children has applied for patents concerning 298, 52, and 80 mAbs and the MB platform technology that are related to this work: 63/496,136 – Multabody constructs, compositions, and methods targeting sarbecoviruses; and PCT/CA2022/051517 – Modified Multabody constructs, compositions, and methods targeting SARS-CoV-2. B.T. and J.-P.J. are founders of Radiant Biotherapeutics and are members of its Scientific Advisory Board. E.R. and A.J. have previously consulted for Radiant Biotherapeutics. M.S.N., Y.H., and D.D.H. are inventors on patents related to this work: 10-40 and 11-11 mAbs (WO/2023/004431 – Characterization of potent and broadly neutralizing monoclonal antibodies against SARS-COV-2, its variants, and related coronaviruses and methods of use); and 2-7 mAb (WO/2022/232255 – Antibodies for the treatment and prevention of COVID-19 and emerging variants). D.D.H. is a cofounder of TaiMed Biologics and RenBio, a consultant to WuXi Biologics and Brii Biosciences, and a member of the board of directors for Vicarious Surgical. The other authors declare that they have no competing interests. **Data and materials availability:** All data associated with this study are present in the paper or the Supplementary Materials. The electron microscopy maps have been deposited in the Electron Microscopy Data Bank (EMDB) with accession codes EMD-28067 (tri-specific MB, refinement with no symmetry) and EMD-28068 (tri-specific MB, octahedral symmetry). The crystal structure of 80 Fab–RBD has been deposited in the Protein Data Bank (PDB ID: 8DNN). Materials will be made available to the scientific community by contacting the corresponding author and completion of a materials transfer agreement.

Submitted 23 October 2022
Resubmitted 11 February 2022
Accepted 26 April 2023
Published 24 May 2023
10.1126/scitranslmed.adf4549